



Small Scale Low Constraint Fracture Toughness Test Discussion and Analysis

Final Report 277-T-07

For Project

Weld Design, Testing, and Assessment Procedures for High Strength Pipelines

Prepared for the

Design, Materials, and Construction Technical Committee of
Pipeline Research Council International, Inc.
Project MATH-1 Catalog No. L5XXXX

and

U.S. Department of Transportation
Pipeline and Hazardous Materials Safety Administration
Office of Pipeline Safety
Agreement Number DTPH56-07-T-000005

Prepared by

D.Y. Park, W.R. Tyson, J.A. Gianetto, G. Shen and R.S. Eagleson
CANMET Materials Technology Laboratory

E. Lucon and T.S. Weeks
National Institute of Standards and Technology

September 2011

This research was funded in part under the Department of Transportation, Pipeline and Hazardous Materials Safety Administration's Pipeline Safety Research and Development Program. The views and conclusions contained in this document are those of the authors and should not be interpreted as representing the official policies, either expressed or implied, of the Pipeline and Hazardous Materials Safety Administration, or the U.S. Government.

Contribution of an agency of the U.S. government, not subject to copyright

CANMET Materials Technology Laboratory

Small Scale Low Constraint Fracture Toughness Test Discussion and Analysis

D.Y. Park, W.R. Tyson, J.A. Gianetto, G. Shen and R.S. Eagleson
CANMET Materials Technology Laboratory
Minerals and Metals Sector, Natural Resources Canada
183 Longwood Road South, Hamilton, ON, Canada, L8P 0A5

E. Lucon and T.S. Weeks
*National Institute of Standards and Technology

CANMET Report No. 2010-29(TR)

September 2011

Disclaimer

Natural Resources Canada makes no representations or warranties respecting the contents of this report, either expressed or implied, arising by law or otherwise, including but not limited to implied warranties or conditions of merchantability or fitness for a particular purpose.



CATALOG NO. L5XXXX

Small Scale Low Constraint Fracture Toughness Test Discussion and Analysis

Final Report 277-T-07

For Project

Weld Design, Testing, and Assessment Procedures for High Strength Pipelines

Prepared for the

Design, Materials, and Construction Technical Committee of Pipeline Research Council International, Inc.
Project MATH-1 Catalog No. L5XXXX

and

U.S. Department of Transportation
Pipeline and Hazardous Materials Safety Administration
Office of Pipeline Safety
Agreement Number DTPH56-07-T-000005

Prepared by

D.Y. Park, W.R. Tyson, J.A. Gianetto, G. Shen and R.S. Eagleson
CANMET Materials Technology Laboratory

E. Lucon and T.S. Weeks
National Institute of Standards and Technology

September 2011

Version	Date of Last Revision	Date of Uploading	Comments
Draft	June 2011	June 2011	
Final	October 2011	December 2011	

This report is furnished to Pipeline Research Council International, Inc. (PRCI) under the terms of PRCI contract [277-PR-348-074512], between PRCI and the MATH-1 contractors:

- Electricore (prime contractor),
- Center for Reliable Energy Systems, CANMET, NIST, and The Lincoln Electric Company (sub-contractors).

The contents of this report are published as received from the MATH-1 contractor and subcontractors. The opinions, findings, and conclusions expressed in the report are those of the authors and not necessarily those of PRCI, its member companies, or their representatives. Publication and dissemination of this report by PRCI should not be considered an endorsement by PRCI of the MATH-1 contractor and subcontractors, or the accuracy or validity of any opinions, findings, or conclusions expressed herein.

In publishing this report, PRCI and the MATH-1 contractors make no warranty or representation, expressed or implied, with respect to the accuracy, completeness, usefulness, or fitness for purpose of the information contained herein, or that the use of any information, method, process, or apparatus disclosed in this report may not infringe on privately owned rights. PRCI and the MATH-1 contractors assume no liability with respect to the use of, or for damages resulting from the use of, any information, method, process, or apparatus disclosed in this report. By accepting the report and utilizing it, you agree to waive any and all claims you may have, resulting from your voluntary use of the report, against PRCI and the MATH-1 contractors.

Pipeline Research Council International Catalog No. L5XXXX

PRCI Reports are Published by Technical Toolboxes, Inc.

3801 Kirby Drive, Suite 520
Houston, Texas 77098
Tel: 713-630-0505
Fax: 713-630-0560
Email: info@ttoolboxes.com

PROJECT PARTICIPANTS

PROJECT TEAM MEMBER	COMPANY AFFILIATION	PROJECT TEAM MEMBER	COMPANY AFFILIATION
Arti Bhatia	Alliance	Jim Costain	GE
Jennifer Klementis	Alliance	Gilmar Batista	Petrobras
Roger Haycraft	Boardwalk	Marcy Saturno de Menezes	Petrobras
David Horsley	BP	Dave Aguiar	PG&E
Mark Hudson	BP	Ken Lorang	PRCI
Ron Shockley	Chevron	Maslat Al-Waranbi	Saudi Aramco
Sam Mishael	Chevron	Paul Lee	SoCalGas
David Wilson	ConocoPhillips	Alan Lambeth	Spectra
Satish Kulkarni	El Paso	Robert Turner	Stupp
Art Meyer	Enbridge	Gilles Richard	TAMSA
Bill Forbes	Enbridge	Noe Mota Solis	TAMSA
Scott Ironside	Enbridge	Philippe Darcis	TAMSA
Sean Keane	Enbridge	Dave Taylor	TransCanada
Laurie Collins	Evraz	Joe Zhou	TransCanada
David de Miranda	Gassco	Jason Skow	TransGas
Adriaan den Herder	Gasunie	Ernesto Cisneros	Tuberia Laguna
Jeff Stetson	GE	Vivek Kashyap	Welpsun
		Chris Brown	Williams

CORE RESEARCH TEAM	
RESEARCHER	COMPANY AFFILIATION
Yaoshan Chen	Center for Reliable Energy Systems
Yong-Yi Wang	Center for Reliable Energy Systems
Ming Liu	Center for Reliable Energy Systems
Dave Fink	Lincoln Electric Company
Marie Quintana	Lincoln Electric Company
Vaidyanath Rajan	Lincoln Electric Company
Joe Daniel	Lincoln Electric Company
Radhika Panday	Lincoln Electric Company
James Gianetto	CANMET Materials Technology Laboratory
John Bowker	CANMET Materials Technology Laboratory
Bill Tyson	CANMET Materials Technology Laboratory
Guowu Shen	CANMET Materials Technology Laboratory
Dong Park	CANMET Materials Technology Laboratory
Timothy Weeks	National Institute of Standards and Technology
Mark Richards	National Institute of Standards and Technology
Dave McColskey	National Institute of Standards and Technology
Enrico Lucon	National Institute of Standards and Technology
John Hammond	Consultant Metallurgist & Welding Engineer

This Page Intentionally Left Blank

FINAL REPORT STRUCTURE

Focus Area 1 - Update of Weld Design, Testing, and Assessment Procedures for High Strength Pipelines		
Report #	Description	Lead Authors
277-T-01	Background of Linepipe Specifications	CRES/CANMET
277-T-02	Background of All-Weld Metal Tensile Test Protocol	CANMET/Lincoln
277-T-03	Development of Procedure for Low-Constraint Toughness Testing Using a Single-Specimen Technique	CANMET/CRES
277-T-04	Summary of Publications: Single-Edge Notched Tension SE(T) Tests	CANMET
277-T-05	Small Scale Tensile, Charpy V-Notch, and Fracture Toughness Tests	CANMET/NIST
277-T-06	Small Scale Low Constraint Fracture Toughness Test Results	CANMET/NIST
277-T-07	Small Scale Low Constraint Fracture Toughness Test Discussion and Analysis	CANMET/NIST
277-T-08	Summary of Mechanical Properties	CANMET
277-T-09	Curved Wide Plate Tests	NIST/CRES
277-T-10	Weld Strength Mismatch Requirements	CRES/CANMET
277-T-11	Curved Wide Plate Test Results and Transferability of Test Specimens	CRES/CANMET
277-S-01	Summary Report 277 Weld Design, Testing, and Assessment Procedures for High Strength Pipelines	CRES

Focus Area 2 - Development of Optimized Welding Solutions for X100 Linepipe Steel		
Report #	Description	Lead Authors
278-T-01	State of The Art Review	Lincoln
278-T-02	Material Selection, Welding and Weld Monitoring	Lincoln/CANMET
278-T-03	Microstructure and Hardness Characterization of Girth Welds	CANMET/Lincoln
278-T-04	Microstructure and Properties of Simulated Weld Metals	CANMET/Lincoln
278-T-05	Microstructure and Properties of Simulated Heat Affected Zones	CANMET/Lincoln
278-T-06	Essential Welding Variables	Lincoln/CANMET
278-T-07	Thermal Model for Welding Simulations	CRES/CANMET
278-T-08	Microstructure Model for Welding Simulations	CRES/CANMET
278-T-09	Application to Other Processes	Lincoln/CANMET
278-S-01	Summary Report 278 Development of Optimized Welding Solutions for X100 Line Pipe Steel	Lincoln

EXECUTIVE SUMMARY

This is the sixth report of a series of seven reports detailing the small-scale mechanical testing performed on the baseline welds in this consolidated program. An outline of the reporting flow is given in the Introduction to the Summary of Mechanical Properties report 277-T-08. This report summarizes and discusses the toughness results of the previous report 277-T-06.

Extensive single edged notched tension and bending (SE(T) and SE(B)) tests were performed to apply the SE(T) procedure developed at CANMET as well as standard SE(B) procedures to pipeline girth welds as a contribution to a broader project on strain-based design (SBD) for pipeline girth weld integrity. This report presents discussions and recommendations related to the results which are reported separately. Conclusions are as follows:

1. Surface notched specimens produced relatively straight fatigue crack fronts both without (round 1 & round 2) and with (round 3) local compression prior to precracking.
2. The optimal side grooves were 15 %B (depth of 7.5 %B on each side), where B is the thickness of the specimen. A total side-grooving depth of 10 % (5 %B on each side) was used for round 3 specimens and appears to have little or no effect on test results, as confirmed by the comparison with one plane-sided SE(T) specimen.
3. Resistance R curves for weld metal (WM) were lower than those for base metal (BM) or heat-affected zone (HAZ) specimens, even though the WM overmatched the BM. Toughness properties for round 3 welds were superior to those for rounds 1 and 2 weld metals, although a difference in pipe wall thickness could moderate this conclusion.
4. Power-law regression curves generated for data between exclusion lines (following ASTM procedures) adequately represented data measured for significantly larger crack growth, *i.e.*, within 10 % error for an approximate doubling of crack growth.
5. Toughness of BM, HAZ and WM increased significantly with decreases in initial crack length, although R-curves for dual-torch WM (R2) were relatively insensitive to initial crack length.
6. In an overmatched weld notched in the HAZ, asymmetric deformation occurs at the crack tip and leads to biased crack growth and discrepancy in crack length measurements on the BM and WM sides. The crack grows toward the lower-strength base metal, and the change in crack length Δa tends to be larger on the WM side for overmatched welds.

TABLE OF CONTENTS

EXECUTIVE SUMMARY	viii
TABLE OF CONTENTS	ix
LIST OF FIGURES	x
LIST OF TABLES	xii
1 INTRODUCTION	1
2 OBJECTIVES	1
3 MATERIAL, SPECIMENT PREPARTION, AND TESTING	1
3.1 Material Properties and Specimen Preparation	1
3.2 Fatigue Precracking—Local Compression	3
3.3 SE(T) Testing	8
3.4 SE(B) testing	10
4 RESULTS	12
4.1 Resistance Curves	12
4.2 Post-test Analysis	31
4.3 SE(T) Test Comparison: Single- vs. Multi-specimen	33
4.4 Validation of Power-law Regression	35
4.5 Effects of Material, Constraint and Temperature	36
4.6 Asymmetrical Deformation of HAZ Specimens	42
5 CONCLUSIONS	47
6 ACKNOWLEDGEMENTS	47
7 REFERENCES	48

LIST OF FIGURES

Figure 1. X100 rolled welds: (a) single-torch (round 1) and (b) dual-torch (round 2).....	2
Figure 2. Targeted precrack locations: (a) weld metal centerline and (b) HAZ region (solid line: 3 mm precrack and dotted line: 6 mm precrack).	3
Figure 3. Effect of local compression on crack front straightness of through-thickness-notched B × 2B (B = 17.2 mm) SE(B) specimens: (a) without local compression and (b) with local compression. Scale in (a) is the same as that in (b).	4
Figure 4. Effect of local compression on applied load of through-thickness notched B×2B (B = 17.2 mm) SE(B) specimens.	4
Figure 5. Effect of local compression on J-resistance curve of through-thickness notched B×2B (B = 17.2 mm) SE(B) specimens.	5
Figure 6. Examples of inner diameter (ID) surface notched SE(T) specimens without local compression prior to precracking: (a) $a_o = 5.1$ mm and (b) $a_o = 7.0$ mm. Finest scale graduations are 1 mm.	5
Figure 7. Fracture surfaces of round 3 HAZ SE(B) specimens DH1 (a) and DH6 (b), without and with local compression respectively. Scale graduations are 0.5 mm.....	6
Figure 8. SE(T) test setup: (a) room temperature and (b) low temperature.	10
Figure 9. SE(B) test setup at CANMET (HAZ region, target $a_o = 6$ mm, specimen BHZRTG04)).	12
Figure 10. Load-CMOD curves for SE(T) specimens, B=W=17.5 mm.	13
Figure 11. An example of apparent negative crack growth and calculation of a_{oq} determined with and without negative crack growth data. This example is obtained from another study; pronounced negative crack growth like this example was not observed in this study.	14
Figure 12. Power-law fitting parameters (a) $C1$ and (b) $C2$ of $J = C1\Delta a^{C2}$, fit with an assumed linear dependence on the initial crack length a_{oq} to enable small interpolation/extrapolation to target crack size. J is in kJ/m^2 . Examples are shown for room temperature SE(T) tests on base metal (BM).	16
Figure 13. SE(T) J-resistance curves extrapolated/interpolated for the target crack lengths (3 mm and 6 mm), calculated with the $C1$ and $C2$ power-law parameters fit to a linear dependence on a/W or averaged: (a) RT, $a_o = 3$ mm, (b) -20 °C, $a_o = 3$ mm, (c) RT, $a_o = 6$ mm and (d) -20 °C, $a_o = 6$ mm. Owing to lack of data, fits of the parameters as a function of a/W were not obtained for base metal and HAZ (round 2).	20
Figure 14. SE(B) J-resistance curves extrapolated/interpolated for the target crack lengths (3 mm and 6 mm) calculated with the $C1$ and $C2$ power-law parameters fit to a linear dependence on a/W or averaged: (a) RT, $a_o = 3$ mm, (b) -20 °C, $a_o = 3$ mm, (c) RT, $a_o = 6$ mm and (d) -20 °C, $a_o = 6$ mm. Owing to lack of data, fits of the parameters as a function of a/W were not obtained for base metal (round 1 & round 2) and HAZ (round 2 and round 3).	22
Figure 15. SE(T) J-resistance curves from experimental measurements of single-torch welds (WMC and HAZ regions) at test temperature of -40 °C (symbols: raw data, lines: fitting curves).	23
Figure 16. SE(T) CTOD-resistance curves extrapolated/interpolated for the target crack lengths (3 mm and 6 mm) with the $C1$ and $C2$ power-law parameters fit to a linear dependence on a/W or averaged: (a) RT, $a_o = 3$ mm, (b) -20 °C, $a_o = 3$ mm, (c) RT, $a_o = 6$ mm and (d) -20 °C, $a_o = 6$ mm. Owing to lack of data, fits of the parameters as a function of a/W were not obtained for base metal and HAZ (round 2).	27
Figure 17. SE(B) CTOD-resistance curves extrapolated/interpolated for the target crack lengths (3 mm and 6 mm) with the $C1$ and $C2$ power-law parameters fit to a linear dependence on a/W or averaged: (a) RT, $a_o = 3$ mm, (b) -20 °C, $a_o = 3$ mm, (c) RT, $a_o = 6$ mm and (d) -20 °C, $a_o = 6$ mm.	

Owing to lack of data, fits of the parameters as a function of a/W were not obtained for base metal (round 1 & round 2) and HAZ (round 2).....	29
Figure 18. SE(T) CTOD-resistance curves from experimental measurements of single-torch welds (WMC and HAZ regions) at test temperature of $-40\text{ }^{\circ}\text{C}$	30
Figure 19. Representative fracture surfaces of SE(T) base metal specimens from rounds 1 and 2 (side grooving: 15 % and 20 %).	32
Figure 20. Representative fracture surfaces of SE(B) base metal specimens from round 3 (side grooving: 10 %). Scale graduations equal 0.5 mm.	32
Figure 21. Comparison between plane-sided (1 specimen) and 10 % side-grooved (5 specimens) SE(T) test results for WM (round 3).	33
Figure 22. Comparisons of J-resistance curves from SE(T) multi-specimen and single-specimen techniques.	34
Figure 23. Comparisons of regression methods with measurements for single-torch weld metal centerline specimens ($a_o = 4\text{ mm}$): (a) J-resistance curve and (b) CTOD-resistance curve (Symbols: calculations from unloading compliance measurements; solid lines: regressions). The solid symbol (near $\delta = 0.25\text{ mm}$) corresponds to the maximum force attained during the test.	36
Figure 24. Optical microscope images of etched mid-thickness sections of SE(T) specimens: weld metal centerline specimen (WMLTK14) [(a) and (b)] and HAZ specimen (HZLTK17) [(c) and (d)], (b) and (d) show enlarged images near the crack tip of (a) and (c), respectively, and large voids are marked by “V” in the figures.	37
Figure 25. J and CTOD values at $\Delta a = 0.5\text{ mm}$ for SE(T): (a) J-resistance and (b) CTOD-resistance. ...	38
Figure 26. J and CTOD values at $\Delta a = 2\text{ mm}$ for SE(T): (a) J-resistance and (b) CTOD-resistance.	39
Figure 27. J and CTOD values at $\Delta a = 0.5\text{ mm}$ for SE(B): (a) J-resistance and (b) CTOD-resistance	40
Figure 28. J and CTOD values at $\Delta a = 2\text{ mm}$ for SE(B): (a) J-resistance and (b) CTOD-resistance.	41
Figure 29. Deformation behaviors during SE(T) testing at CANMET: (a) symmetrical deformation of base metal specimen ($a_o \approx 6\text{ mm}$) at $\Delta a \approx 2.5\text{ mm}$ and (b) asymmetrical deformation between the upper half (WM side) and the lower half (BM side) of a dual-torch weld HAZ specimen ($a_o \approx 3\text{ mm}$) at $\Delta a \approx 2.2\text{ mm}$	43
Figure 30. Examples of fracture surfaces of SE(T) specimens: single-torch weld, nominal $a_o \approx 3\text{ mm}$, notched at weld metal centerline (WM) (a) crack plane and (b) side view, and at HAZ (c) crack plane and (d) side view.	44
Figure 31. Effect of overmatching WM for surface notched HAZ specimens: compliance-predicted versus optical crack length measurements of (a) Base metal side and (b) Weld metal side. (Bracketed numbers give optical and compliance measurements, respectively.)	45
Figure 32. An example of asymmetrical deformation, during SE(B) testing, around the crack tip ($a_o \approx 3\text{ mm}$) precracked in the HAZ region of single-torch weld metal specimen: (a) at $\Delta a \approx 2.4\text{ mm}$ and (b) after completion of test.	46
Figure 33. J-resistance curve of a SE(T) HAZ specimen (HZR TK21) carried to exceptionally long crack growth at room temperature.	46

LIST OF TABLES

Table 1. Room temperature yield and ultimate tensile strengths of X100 pipe steel and weld metal.	3
Table 2. Assessment of crack size qualification for SE(T) specimens.	7
Table 3. Assessment of crack size qualification for SE(B) specimens.	8
Table 4. SE(T) test matrix for X100 base metal.	8
Table 5. SE(T) test matrix for single-torch X100 rolled welds (round 1).	9
Table 6. SE(T) test matrix for dual-torch X100 rolled welds (round 2).	9
Table 7. SE(T) test matrix for single-torch X100 5G welds (round 3).	9
Table 8. SE(B) test matrix for base metal.	10
Table 9. SE(B) test matrix for single-torch X100 rolled welds (round 1).	11
Table 10. SE(B) test matrix for single-torch X100 rolled welds (round 2).	11
Table 11. SE(B) test matrix for single-torch X100 5G welds (round 3).	11
Table 12. Power-law fitting parameters $C1$ and $C2$ extrapolated/interpolated to the target initial crack lengths ($a = 3$ mm and 6 mm) by linear fits to the initial crack length a_{oq} for SE(T) J-resistance curves.	17
Table 13. Power-law fitting parameters $C1$ and $C2$ extrapolated/interpolated to the target initial crack lengths ($a = 3$ mm and 6 mm) by linear fits to the initial crack length a_{oq} for SE(B) J-resistance curves.	18
Table 14. Power-law fitting parameters $C1$ and $C2$ extrapolated/interpolated to the target initial crack lengths ($a = 3$ mm and 6 mm) using linear fits to the initial crack length a_{oq} for SE(T) CTOD-resistance curves.	24
Table 15. Power-law fitting parameters $C1$ and $C2$ extrapolated/interpolated to the target initial crack lengths ($a = 3$ mm and 6 mm) by linear fits to the initial crack length a_{oq} for SE(B) CTOD-resistance curves.	25
Table 16. Statistics of brittle fracture at -20 °C.	30

1 INTRODUCTION

This is the sixth report of a series of seven reports detailing the small-scale mechanical testing performed on the baseline welds in this consolidated program. An outline of the reporting flow is given in the Introduction to the Summary of Mechanical Properties report 277-T-08. This report summarizes and discusses the toughness results of the previous report 277-T-06. Single-edge-notched tension (SE(T)) procedures and equations have been developed at CANMET to calculate the J-integral and J-/crack-tip-opening displacement (CTOD) -resistance curve with the use of the unloading compliance technique for a clamped SE(T) specimen [1-3]. The present work was done to extend the procedure to pipeline girth welds and to provide data for development of strain-based design for pipeline girth weld integrity assessment. Extensive SE(T) and single-edge-notch bend (SE(B)) testing was performed according to the CANMET SE(T) procedure [2] and to ASTM E1820 [4], respectively. Detailed experimental data and results are reported separately [5]. This report has been prepared to present discussions and recommendations related to those results.

2 OBJECTIVES

The principal objectives of the work were to:

- (1) Apply the SE(T) procedure developed at CANMET to pipeline girth welds (base metal (BM), heat-affected zone (HAZ) and weld metal (WM) centerline regions), and
- (2) Evaluate in detail the results presented in the separate report [5].

3 MATERIAL, SPECIMEN PREPARATION, AND TESTING

3.1 Material Properties and Specimen Preparation

Relevant material property data for the X100 pipe steel and a description of the welding procedures employed to produce the experimental X100 mechanized rolled welds and their corresponding mechanical properties are available in the Report 277-T-05 [6]. The following information relates to the preparation of fracture specimens from the X100 pipe steel and the experimental single and dual-torch welds.

- Pipe material: pipes of X100 (Grade 690), 914 mm (36 in) diameter by 19.1 mm (0.75 in) wall thickness (rounds 1 and 2) and 1067 mm (42 in) by 14.3 mm (0.563 in) wall thickness (round 3).
- Welds: single-torch (round 1) and dual-torch (round 2) rolled girth welds (BM, HAZ & WM regions) (Figure 1); single-torch 5G girth welds (round 3)
- Specimen length: ~345 mm with distance between grips (daylight) $H = 10W = 172$ mm for SE(T) and span $S = 4W$ for SE(B) (round 1 and round 2); ~240 mm with daylight $H = 10W = 118$ mm (round 3)
- Specimen length direction: longitudinal to pipe axis (transverse to weld)

- Cross-section: $\approx 17.5 \text{ mm} \times 17.5 \text{ mm}$ for base metal and dual-torch welds (WM and HAZ) and $17.2 \text{ mm} \times 17.2 \text{ mm}$ for single-torch welds (round 1 and round 2); for round 3, $\approx 14 \text{ mm} \times 14 \text{ mm}$ (BM) and $12.5 \text{ mm} \times 12.5 \text{ mm}$ (WM and HAZ) for SE(B) specimens, $11.8 \text{ mm} \times 11.8 \text{ mm}$ (WM and HAZ) for SE(T) specimens
- Side-groove details: 45° included angle with 0.5 mm radius; total depth of 15 % (7.5 % on each side) for rounds 1 and 2; total depth of 10 % (5 % on each side) for round 3
- Targeted fatigue precrack depths: 3 mm and 6 mm (Figure 2)
- Fatigue precrack: from inner diameter (ID) surface of the pipe
- Test temperatures: room temperature, $-20 \text{ }^\circ\text{C}$, and $-40 \text{ }^\circ\text{C}$
- Local compression: No (rounds 1 and 2); Yes (round 3)
- Material properties are summarized in Table 1. For HAZ region tests, the calculation of fracture toughness values (J and CTOD) was based on the tensile properties of the weld metal. The material properties at $-20 \text{ }^\circ\text{C}$ and $-40 \text{ }^\circ\text{C}$ were inferred from the properties in Table 1, from the equation in British Standard (BS) 7448: Part 2 [7].

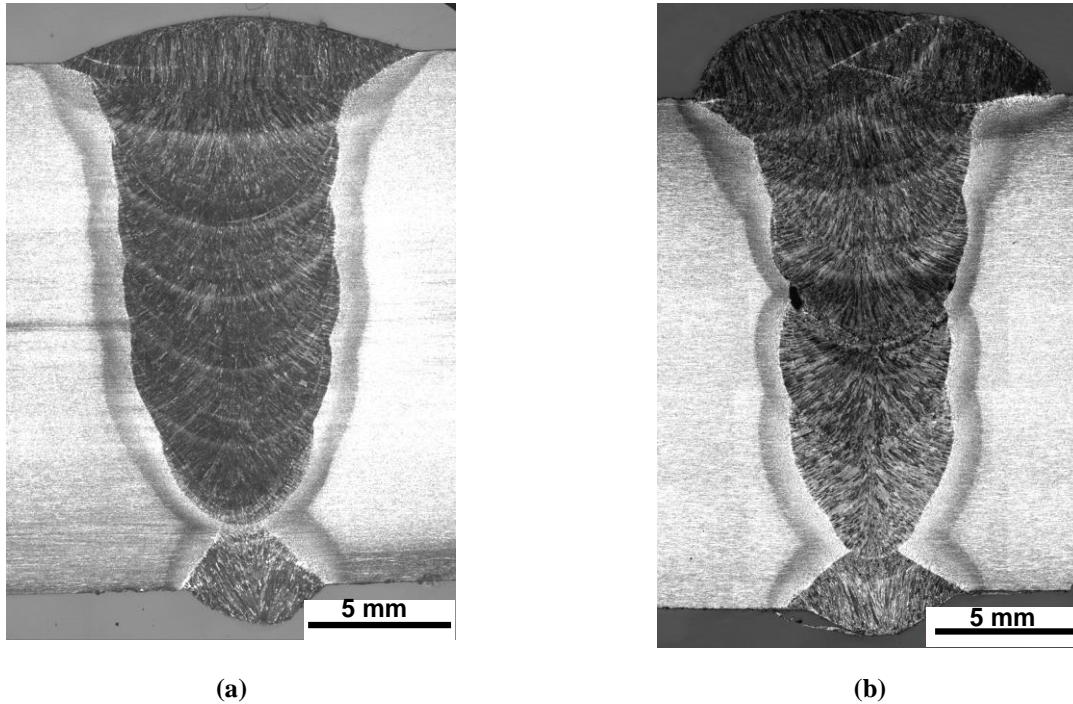


Figure 1. X100 rolled welds: (a) single-torch (round 1) and (b) dual-torch (round 2).

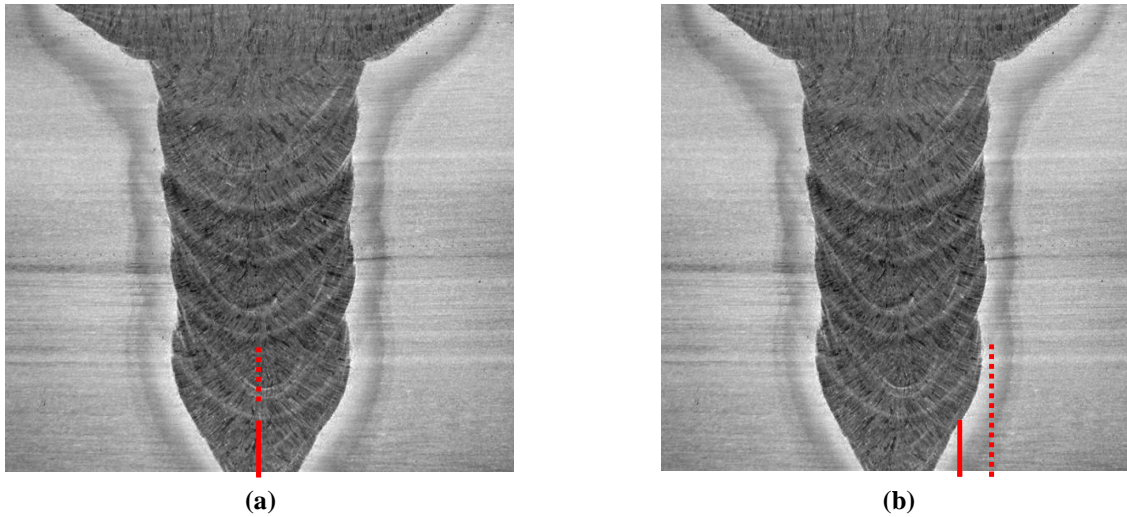


Figure 2. Targeted precrack locations: (a) weld metal centerline and (b) HAZ region (solid line: 3 mm precrack and dotted line: 6 mm precrack).

Table 1. Room temperature yield and ultimate tensile strengths of X100 pipe steel and weld metal.

Material	YS (0.2 %) MPa	UTS MPa
Base metal (rounds 1 and 2)	720	830
Single-torch weld metal (round 1)	825	915
Dual-torch weld metal (round 2)	827	889
Base metal (round 3 – pipe A)	648	807
Base metal (round 3 – pipe B)	710	800
Single-torch weld metal (round 3, 952-D)	843 (*)	915 (*)
Single-torch weld metal (round 3, 952-F)	758 (*)	908 (*)

Notes: YS: yield strength, UTS: ultimate tensile strength
 X100 pipe steel tested using strap tensile specimen parallel to pipe axis
 All-weld-metal strip specimen cut from girth weld
 (*) Average of three clock positions (12:00, 3:00, 6:00)

3.2 Fatigue Precracking—Local Compression

Depending on their magnitude and distribution, residual stresses in the weld metal may cause an uneven fatigue crack front, such as in Figure 3(a). This was confirmed in early testing of through-thickness notched SE(B) specimens, where a wavy (uneven) fatigue crack front was obtained. In such cases, application of local compression (indentation) to the ligament below the machined notch is recommended to achieve a straight fatigue crack front [7]. Figure 3(b) shows a relatively straight fatigue crack front resulting from local compression applied prior to fatigue precracking according to the procedure in the BS standard [7]. The total plastic strain of local compression does not usually exceed 1 % of the specimen thickness, so the effect on fracture toughness

measurements is small, especially up to peak load (Figure 4 and Figure 5). Hence, this specimen preparation prior to fatigue precracking is recommended for through-thickness-notched specimens of welds of this pipe material. The results of $B \times 2B$ SE(B) testing (ASTM E1290 Standard CTOD tests) are reported in 277-T-05 [6].

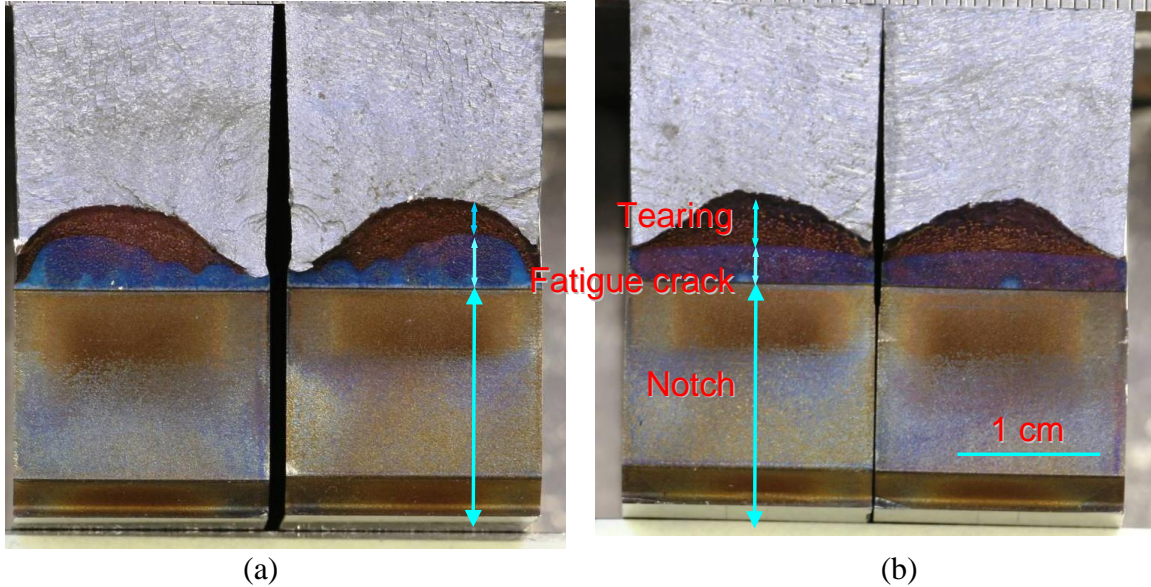


Figure 3. Effect of local compression on crack front straightness of through-thickness-notched $B \times 2B$ ($B = 17.2$ mm) SE(B) specimens: (a) without local compression and (b) with local compression. Scale in (a) is the same as that in (b).

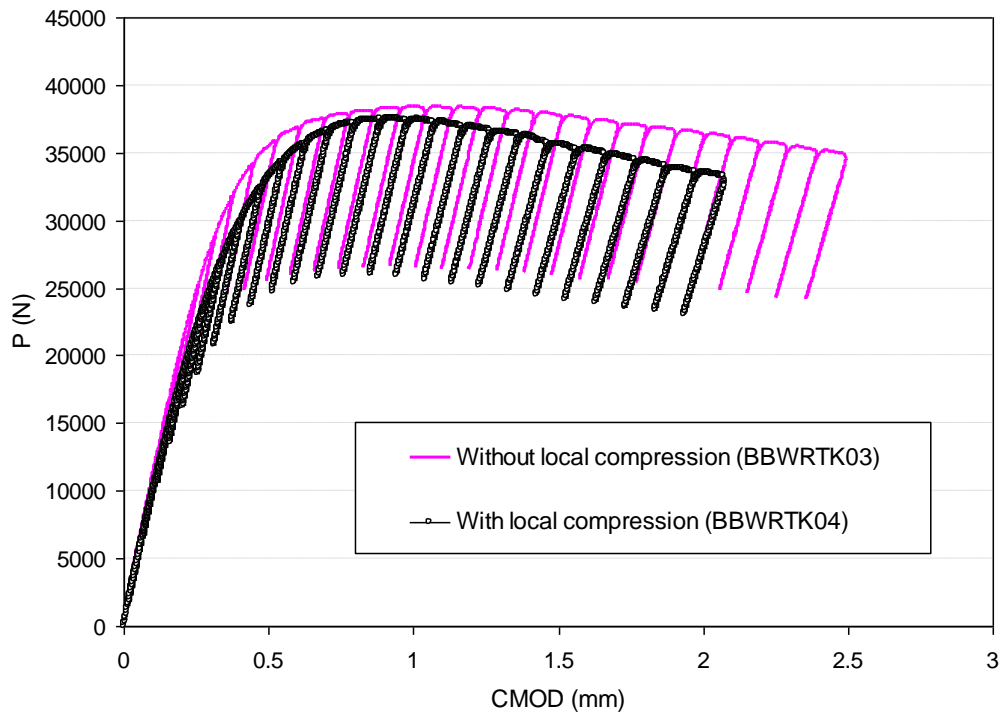


Figure 4. Effect of local compression on applied load of through-thickness notched $B \times 2B$ ($B = 17.2$ mm) SE(B) specimens.

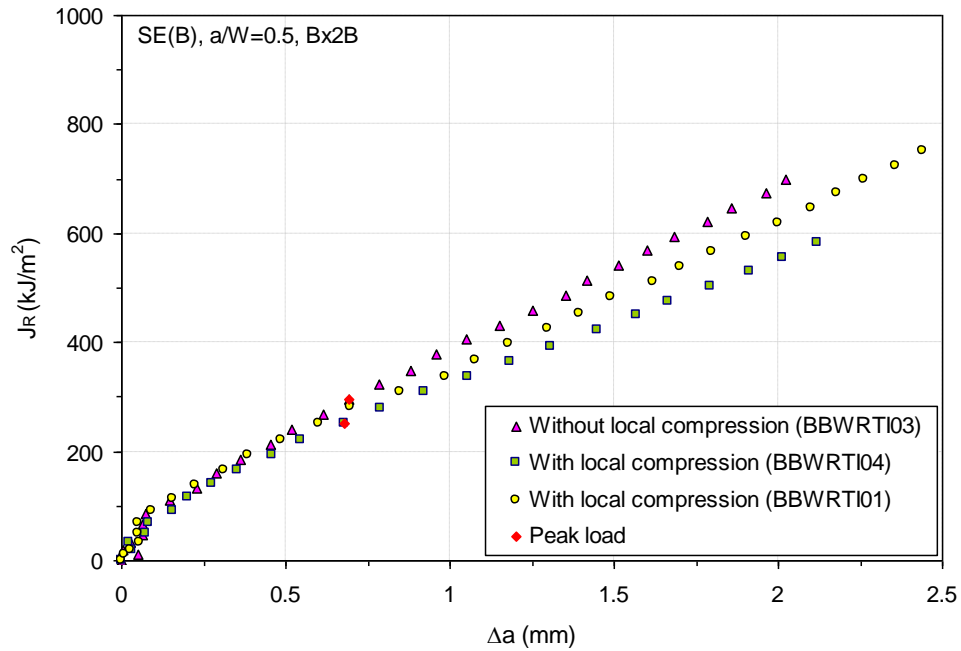


Figure 5. Effect of local compression on J-resistance curve of through-thickness notched B×2B (B = 17.2 mm) SE(B) specimens.

For rounds 1 and 2, surface-notched specimens produced relatively even fatigue crack fronts without local compression prior to precracking (Figure 6). There was some “bowing,” but in most cases the fatigue crack front straightness requirements of the ASTM and BS standards were met. In the case of round 3, however, local compression was applied to all SE(T) and SE(B) specimens of weld metal and HAZ, with the exception of two HAZ SE(B) specimens. The total thickness reduction due to local compression was measured to be in the range 0.06 % - 1.25 % of the original thickness. Comparison between the fracture surfaces of specimen DH1 (without local compression) and DH6 (with local compression), provided in Figure 7, confirms that, even without local compression, relatively straight fatigue crack fronts can be achieved.

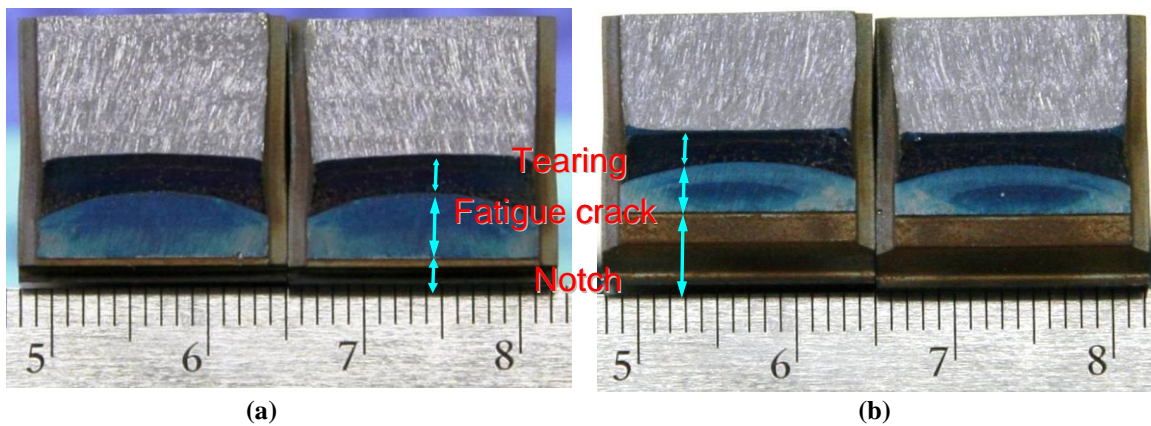


Figure 6. Examples of inner diameter (ID) surface notched SE(T) specimens without local compression prior to precracking: (a) $a_o = 5.1$ mm and (b) $a_o = 7.0$ mm. Finest scale graduations are 1 mm.

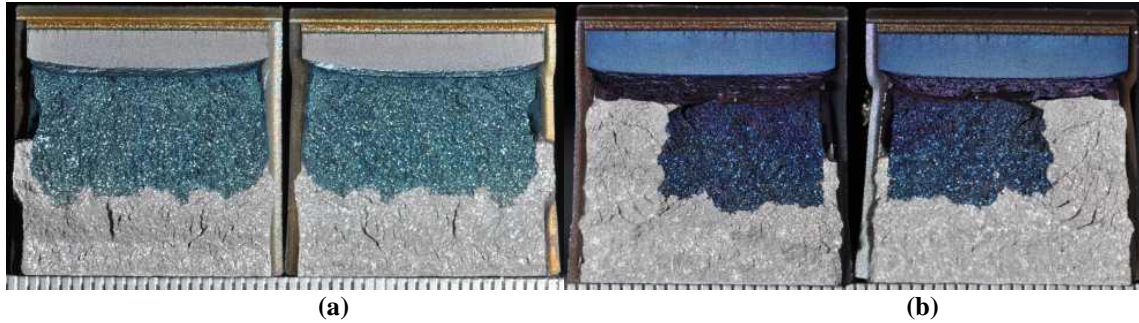


Figure 7. Fracture surfaces of round 3 HAZ SE(B) specimens DH1 (a) and DH6 (b), without and with local compression respectively. Scale graduations are 0.5 mm.

Table 2 and Table 3 summarize the assessment results of crack size qualification according to the requirements of the following standards:

- ASTM E 1820 – 11 [4]:
 - Clause 9.1.4.1 (original crack size): none of the nine physical measurements of initial crack size shall differ by more than 0.05 B from the average a_o
 - Clause 9.1.4.2 (final crack size): none of the nine physical measurements of final physical crack size shall differ by more than 0.05 B from the average a_p
 - Clause 9.1.5.1 (crack extension): none of the nine physical measurements of crack extension shall be less than 50 % of the average crack extension
 - Clause 9.1.5.2 (crack extension prediction): the difference between the unloading compliance predicted crack extension and the measurement shall not exceed $0.15 \Delta_{ap}$ for crack extensions less than $0.2 b_o$ and the difference shall not exceed $0.03 b_o$ thereafter

- BS 7448: Part 2: 1991 [7]:
 - Clause 12.4.1 (original crack size): no two of the inner seven crack length measurements shall differ by more than 20 % a_o .

Crack size assessments of individual specimens are reported separately [5]. In Figure 6 both specimens meet the requirements for fatigue crack front straightness in accordance with BS 7448 Part 2 (for weld metal) clause 12.4.1. However, only the specimen in (b) satisfies the requirements of ASTM E1820 clause 9.1.4.1. This reflects the fact that E1820 is intended for homogeneous materials, whereas BS 7448 Part 2 applies to welds. The complexity of welds makes achievement of a straight crack front considerably more difficult.

Table 2. Assessment of crack size qualification for SE(T) specimens.

Material	Local compression	Target a_o (mm)	Total no. of tested specimens	No. of specimens meeting the requirement*				
				ASTM E1820				BS 7448: Part 2
				9.1.4.1 -original crack size	9.1.4.2 -final crack size	9.1.5.1 -crack extension	9.1.5.2 -crack extension prediction	12.4.1 -original crack size
BM (R1 & R2)	NO	3	3	3 (100)	3 (100)	3 (100)	3 (100)	3 (100)
		6	4	4 (100)	4 (100)	4 (100)	4 (100)	4 (100)
WM (R1)	NO	3	7	0 (0)	6 (86)	7 (100)	7 (100)	3 (43)
		6	5	5 (100)	4(100) [#]	4(100) [#]	4(100) [#]	5 (100)
HAZ (R1) WM side**	NO	3	6	4 (67)	5(100) [#]	5(100) [#]	1(25) [#]	4 (67)
		6	5	5 (100)	5 (100)	5 (100)	4 (80)	5 (100)
HAZ (R1) BM side***	NO	3	6	4 (67)	3 (60) [#]	5(100) [#]	5(100) [#]	4 (67)
		6	5	5 (100)	2 (40)	5 (100)	2 (40)	5 (100)
WM (R2)	NO	3	4	1 (25)	4 (100)	4 (100)	4 (100)	2 (50)
		6	4	4 (100)	3 (75)	4 (100)	3 (75)	4 (100)
HAZ (R2) WM side**	NO	3	4	4 (100)	3 (75)	4 (100)	0 (0)	4 (100)
		6	4	4 (100)	3 (75)	4 (100)	2 (50)	4 (100)
HAZ (R2) BM side***	NO	3	4	4 (100)	2 (50)	4 (100)	4 (100)	3 (75)
		6	4	4 (100)	2 (50)	4 (100)	3 (75)	4 (100)
WM (R3)	YES	3	6	4 (67)	1 (17)	6 (100)	0 (0)	4 (67)
HAZ (R3) WM side**	YES	3	6	5 (83)	0 (0)	2 (33)	0 (0)	5 (83)
HAZ (R3) BM side***	YES	3	6	6 (100)	0 (0)	4 (63)	0 (0)	5 (83)

* Values in parentheses indicate the percentage of specimens satisfying the requirement.

** Assessment of crack size qualification is based on crack measurements on the weld metal side.

*** Assessment of crack size qualification is based on crack measurements on the base metal side.

Final crack length of one specimen was not measured because of fracture.

Table 3. Assessment of crack size qualification for SE(B) specimens.

Material	Local compression	Target a_0 (mm)	Total no. of tested specimens	No. of specimens meeting the requirement*				
				ASTM E1820				BS 7448: Part 2
				9.1.4.1 -original crack size	9.1.4.2 -final crack size	9.1.5.1 -crack extension	9.1.5.2 -crack extension prediction	12.4.1 -original crack size
BM (R1 & R2)	NO	6	2	2 (100)	2 (100)	2 (100)	2 (100)	2 (100)
WM (R1)	NO	3	4	1 (25)	4 (100)	4 (100)	4 (100)	2 (50)
		6	4	1 (25)	4 (100)	4 (100)	4 (100)	4 (100)
HAZ (R1) WM side**	NO	3	3	3 (100)	3 (100)	3 (100)	2 (67)	3 (100)
		6	4	4 (100)	4 (100)	4 (100)	3 (75)	4 (100)
HAZ (R1) BM side***	NO	3	3	3 (100)	3 (100)	3 (100)	3 (100)	3 (100)
		6	4	4 (100)	4 (100)	4 (100)	3 (75)	4 (100)
WM (R2)	NO	3	2	0 (0)	2 (100)	2 (100)	2 (100)	2 (100)
		6	2	2 (100)	2 (100)	2 (100)	2 (100)	2 (100)
BM (R3)	YES	3	5	5 (100)	4 (80)	5 (100)	2 (40)	4 (80)
WM (R3)	YES	3	6	6 (100)	0 (0)	6 (100)	4 (67)	5 (83)
HAZ (R3) WM side**	YES	3	5	5 (100)	4 (80)	4 (80)	3 (60)	5 (100)
HAZ (R3) BM side***	YES	3	5	5 (100)	4 (80)	4 (80)	3 (60)	5 (100)

* Values in parentheses indicate the percentage of specimens satisfying the requirement.

** Assessment of crack size qualification is based on crack measurements on the weld metal side.

*** Assessment of crack size qualification is based on crack measurements on the base metal side.

3.3 SE(T) Testing

A total of 61 SE(T) tests were conducted according to the matrices shown in Table 4 to Table 7. Figure 8 shows test setups at room temperature and low temperatures. For low-temperature testing, a customized liquid-nitrogen environmental chamber was placed between the grips. The temperature measured within the distance of 2B from the notch was stable to ± 2 °C before testing. However, temperature fluctuated up to ± 5 °C, especially at -40 °C, during testing.

Table 4. SE(T) test matrix for X100 base metal.

Temperature, °C	Target Crack Length	Number of specimens (specimen ID)
≈ 20 °C (RT)	a = 3 mm	2 (BMRTK06, -K09)
	a = 6 mm	4 (BMRTK12, -K13, -K14, -K02(20 % SG))
-20 °C	a = 3 mm	1 (BMLTK10)
	a = 6 mm	1 (BMLTK11)

Table 5. SE(T) test matrix for single-torch X100 rolled welds (round 1).

Temperature, °C	Target Crack Length	Number of specimens (specimen ID)	
		WMC	HAZ
≈20 °C (RT)	a = 3 mm	2 (WMRTK01, -K22)	2 (HZRTK07, -K21)
	a = 6 mm	2 (WMRTK11, -K19)	2 (HZRTK18, -K20)
-20 °C	a = 3 mm	3 (WMLTK02, -K15, -K23)	3 (HZLTK08, -K09, -K16)
	a = 6 mm	3 (WMLTK12, -K13, -K14)	3 (HZLTK05, -K06, -K17)
-40 °C	a = 3 mm	2 (WMLT4K24, -K25)	2 (HZLT4K26, -K27)

Table 6. SE(T) test matrix for dual-torch X100 rolled welds (round 2).

Temperature, °C	Target Crack Length	Number of specimens (specimen ID)	
		WMC	HAZ
≈ 20 °C (RT)	a = 3 mm	2 (WMRTF02, -F09)	2 (HZRTF05, -F14)
	a = 6 mm	2 (WMRTF04, -F11)	2 (HZRTF07, -F16)
-20 °C	a = 3 mm	2 (WMLTF10, -F102)	2 (HZLTF06, -F13)
	a = 6 mm	2 (WMLTF03, -F12)	2 (HZLTF08, -F28)

Table 7. SE(T) test matrix for single-torch X100 5G welds (round 3).

Temperature, °C	Target Crack Length	Number of specimens (specimen ID)	
		WMC	HAZ
-20 °C	a = 3 mm	3 (DW1-B, DW3-A, DW6-A)	3 (DH1-A, DH3-A, DH6-A)
		3 (FW1-A, FW3-A, FW6-A)	3 (FH1-A, FH3-A, FH6-A)

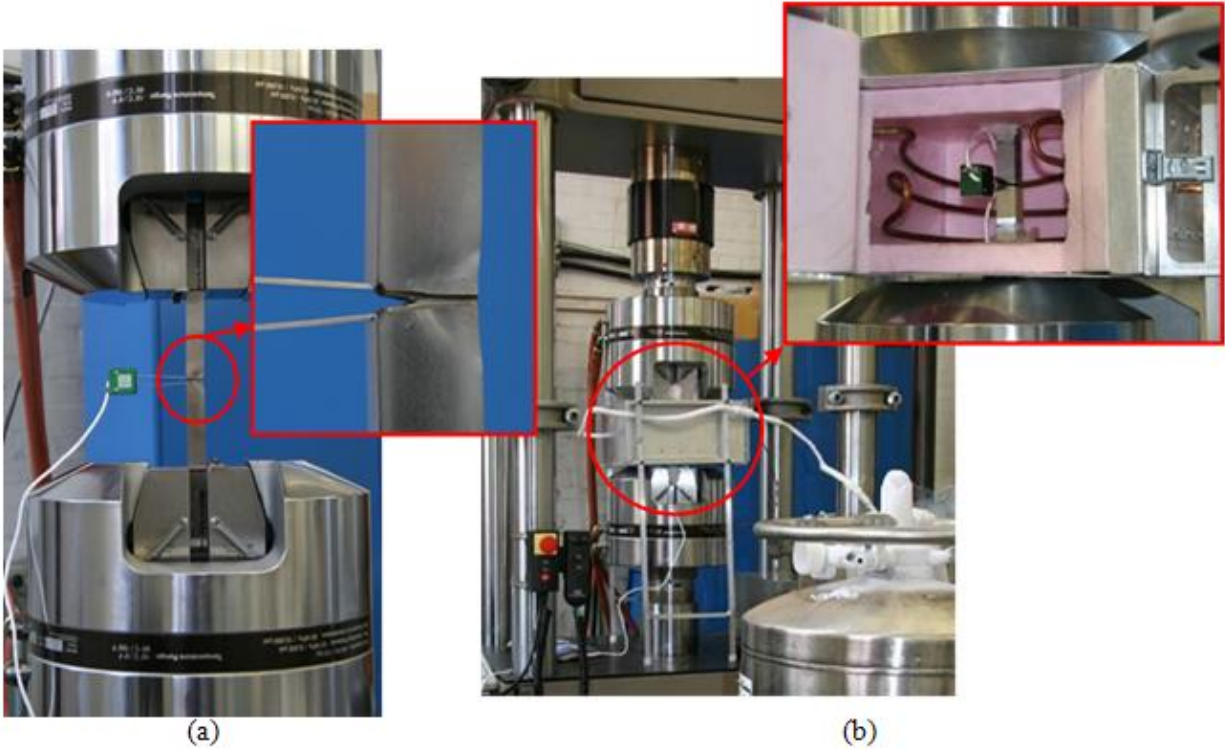


Figure 8. SE(T) test setup: (a) room temperature and (b) low temperature.

3.4 SE(B) testing

A total of 40 SE(B) tests were performed according to the matrices in Table 8 to Table 11 following the procedure of ASTM E1820 [4]. Figure 9 shows an example of SE(B) testing at CANMET. Low-temperature testing was conducted in an environmental chamber, and the stability of temperature was maintained within ± 1 °C (CANMET tests) and ± 2 °C (NIST tests).

Table 8. SE(B) test matrix for base metal.

Temperature, °C	Target Crack Length	Number of specimens (specimen ID)
≈ 20 °C (RT)	a = 6 mm	2 (BBMRT1, -T2)
-20 °C	a = 3 mm	5 (BM2, BM3, BM4, BM5, BM6)

Table 9. SE(B) test matrix for single-torch X100 rolled welds (round 1).

Temperature, °C	Target Crack Length	Number of specimens (specimen ID)	
		WMC	HAZ
≈ 20 °C (RT)	a = 3 mm	2 (BWMRTG05, -I10)	2 (BHZRTI05, -I06)
	a = 6 mm	2 (BWMRTI04, -I11)	2 (BHZRTG04, -I08)
-20 °C	a = 3 mm	2 (BWMLTI01, -I02)	2 (BHZLTI13, -I14)
	a = 6 mm	2 (BWMLTG06, -I12)	2 (BHZLTG08, -I15)

Table 10. SE(B) test matrix for single-torch X100 rolled welds (round 2).

Temperature, °C	Target Crack Length	Number of specimens (specimen ID)	
		WMC	HAZ
≈ 20 °C (RT)	a = 3 mm	1 (BWMRTF21)	1 (BHZLTF25)
	a = 6 mm	1 (BWMRTF23)	
-20 °C	a = 3 mm	1 (BWMLTF22)	1 (BHZLTF26)
	a = 6 mm	1 (BWMLTF24)	

Table 11. SE(B) test matrix for single-torch X100 5G welds (round 3).

Temperature, °C	Target Crack Length	Number of specimens (specimen ID)	
		WMC	HAZ
-20 °C	a = 3 mm	3 (DW1, DW3, DW6) 3 (FW1, FW3, FW6)	2 (DH1, DH6) 3 (FH1, FH3, FH6)

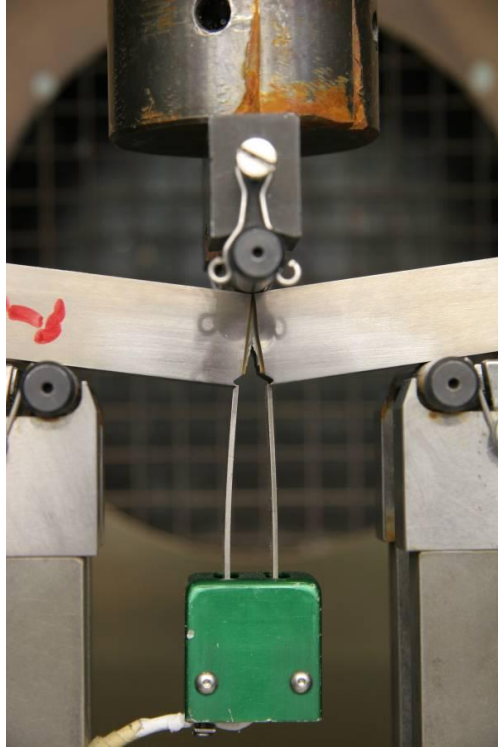


Figure 9. SE(B) test setup at CANMET (HAZ region, target $a_o = 6$ mm, specimen BHZRTG04).

4 RESULTS

4.1 Resistance Curves

Resistance curves were evaluated according to the standard J-integral calculation procedure of ASTM E1820-11 [4] for SE(B) specimens and to the new procedure developed at CANMET for SE(T) specimens [2,3], with the use of CMOD unloading compliance to measure crack length in both cases. Figure 10 shows examples of experimental data (load vs. CMOD) for SE(T) specimens of base metal (BM), weld metal (WM) centerline and HAZ regions. The J- and CTOD-resistance data were curve-fit to power-law regression curves, using data between the 0.15 mm and 1.5 mm exclusion lines, according to the procedure of ASTM E1820:

$$J \text{ or } CTOD = C1\Delta a^{C2}, \quad (1)$$

where J and $CTOD$ are the J-integral and the CTOD converted from the J-integral, respectively, Δa is crack extension, and $C1$ and $C2$ are regression constants.

J- and CTOD-resistance curves and curve-fit parameters for all SE(T) and SE(B) specimens are reported separately [5].

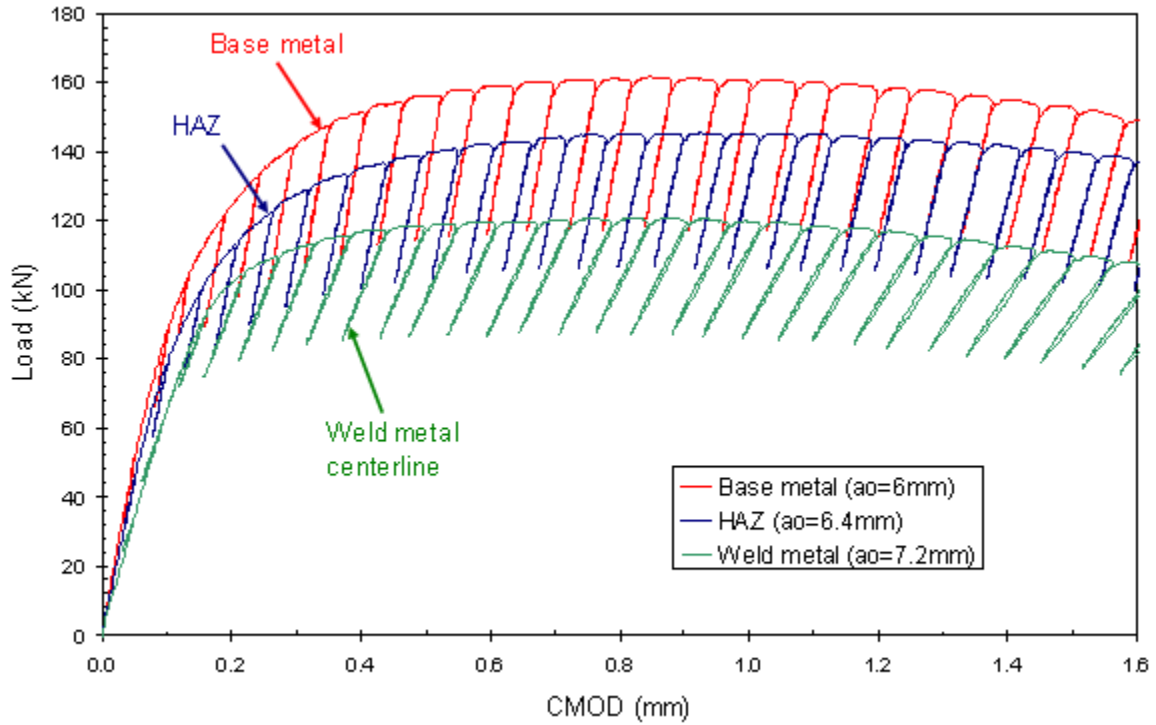


Figure 10. Load-CMOD curves for SE(T) specimens, B=W=17.5 mm.

According to the procedure of ASTM E1820, the initial crack length estimated from unloading compliance should be adjusted. The adjusted initial crack length, a_{oq} , is obtained by identifying all J_i and a_i pairs before maximum load and fitting them to the following equation,

$$a = a_{oq} + \frac{J}{2\sigma_Y} + BJ^2 + CJ^3, \quad (2)$$

where σ_Y is the flow strength (*i.e.*, average of yield and ultimate strengths) and B and C are constants. However, in cases including apparent negative crack growth data, an alternative method was used in this study: initial J_i and a_i pairs up to the maximum negative growth point (*i.e.*, lower part of the nose of J-R curve, *e.g.*, square symbols in Figure 11) were excluded from the above fitting procedure and only the remaining data before maximum load were used. The alternative method generally reduces a_{oq} and results in a better prediction of initial crack length with respect to the measured values, as indicated in Figure 11.

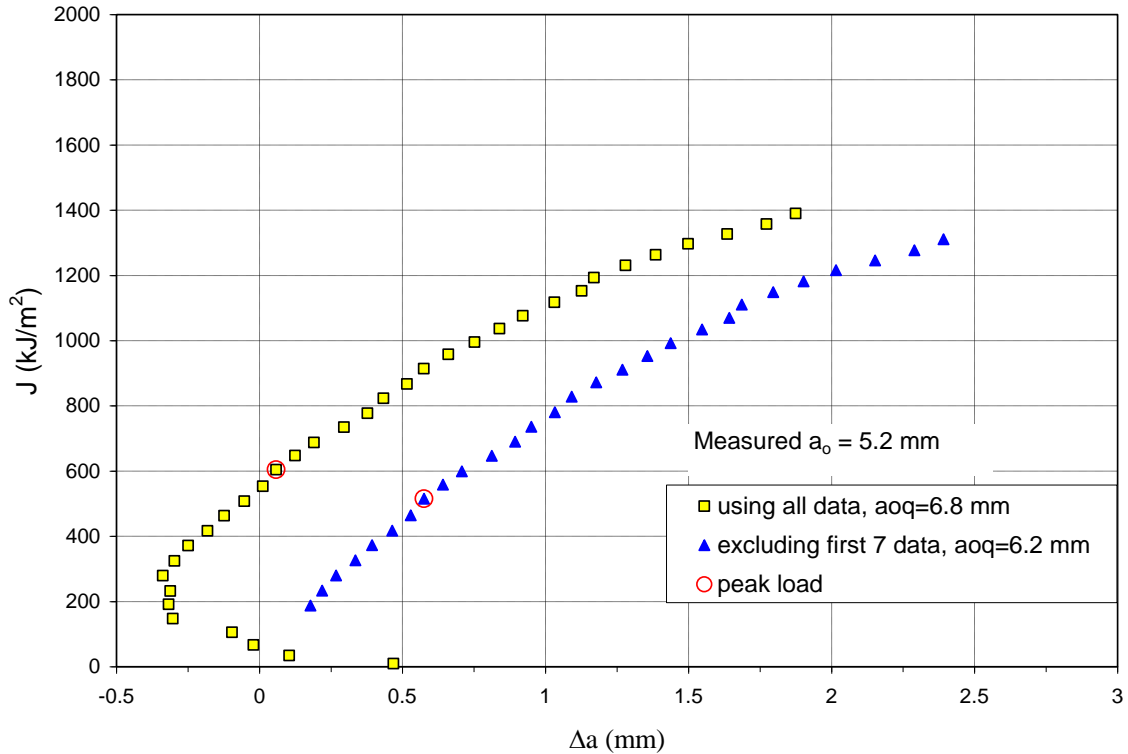


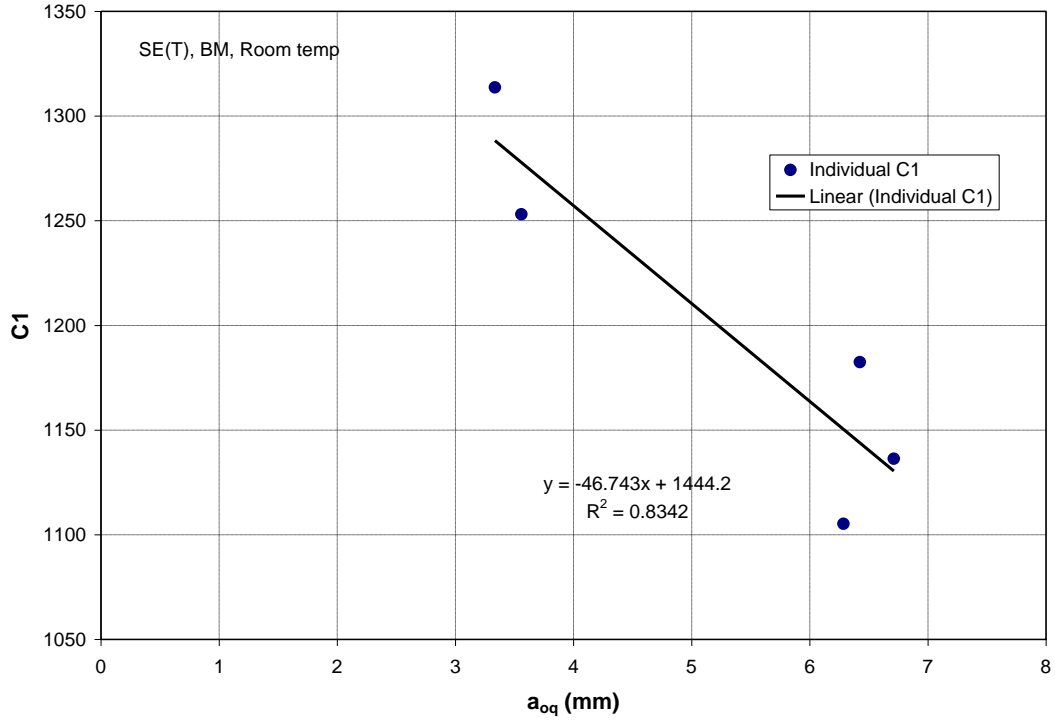
Figure 11. An example of apparent negative crack growth and calculation of a_{oq} determined with and without negative crack growth data. This example is obtained from another study; pronounced negative crack growth like this example was not observed in this study.

4.1.1 J-Resistance Curves

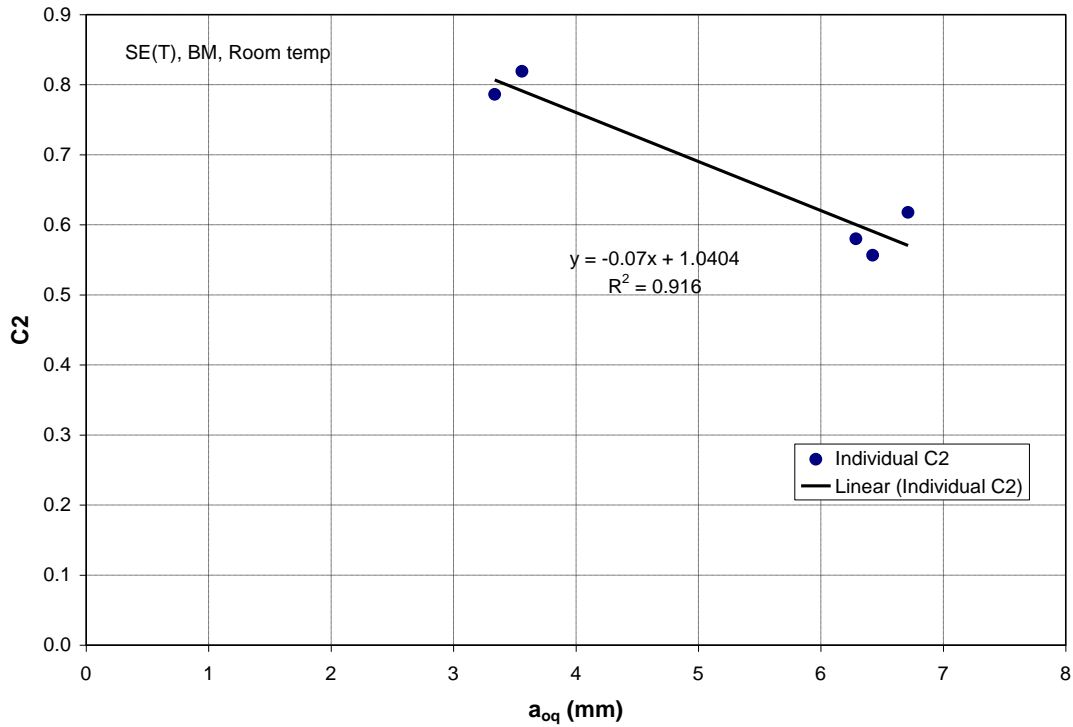
Target initial crack lengths were 3 mm and 6 mm, but actual lengths were a little different. Hence, for round 1 and round 2 tests, the curve-fit parameters were in turn fit to an assumed linear dependence on initial crack length to extrapolate/interpolate them to the target initial crack length values, as seen in the example shown in Figure 12. Conversely, all round 3 test specimens were fatigue precracked to nominally the same initial crack size (~2.6 mm), and therefore the curve-fit parameters obtained from fitting experimental data are not suitable for extrapolation/interpolation. This is also confirmed by the low values obtained for the correlation coefficient R^2 , which range from 0.0002 to 0.49. Hence, for round 3 tests, power-law fitting parameters representing WM and HAZ fracture behavior were obtained by just averaging $C1$ and $C2$ values calculated from individual tests.

Table 12 and Table 13 report power-law fitting parameters $C1$ and $C2$ extrapolated/interpolated to the target initial crack lengths ($a = 3$ mm and 6 mm) by linear fits to the initial crack length a_{oq} , in the case of rounds 1 and 2, or averaged for round 3, for SE(T) and SE(B) J-resistance curves, respectively. This enables comparison with curved wide plate (CWP) test measurements of the actual crack length being performed at the National Institute for Standards and Technology (NIST) for development of a strain-based design procedure. Figure 12 shows the procedure used for rounds 1 and 2 for estimating $C1$ and $C2$; Table 12 (SE(T)) and Table 13 (SE(B)) report the

results. Figure 13 and Figure 14 show J-resistance curves plotted using the fitted/averaged $C1$ and $C2$ power-law parameters for the target initial crack lengths of 3 mm and 6 mm for SE(T) and SE(B) specimens, respectively. As only one specimen was tested for each initial crack length for SE(T) testing at $-40\text{ }^{\circ}\text{C}$, raw data and their power-law fitting curves for each crack length are presented for comparison in Figure 15. In general, the J-resistance curves of WM (single and dual-torch) lie well below those of base metal and HAZ regions for both SE(T) and SE(B) specimens. BM curves are generally slightly above HAZ curves, except at small crack growths for SE(T) with $a = 3\text{ mm}$. At $-20\text{ }^{\circ}\text{C}$, the fracture resistance of the weld metal from round 3 is higher than WM from rounds 1 and 2 when SE(T) specimens are used, although it should be noted that the specimen widths differ and this will probably influence the results. The J values measured in this report do not generally satisfy the usual size requirements for size-independent toughness measurements (see, e.g., [4]), and so they are expected to be dependent on geometry (e.g. width W).



(a)



(b)

Figure 12. Power-law fitting parameters (a) $C1$ and (b) $C2$ of $J = C1\Delta a^{C2}$, fit with an assumed linear dependence on the initial crack length a_{oq} to enable small interpolation/extrapolation to target crack size. J is in kJ/m^2 . Examples are shown for room temperature SE(T) tests on base metal (BM).

Table 12. Power-law fitting parameters $C1$ and $C2$ extrapolated/interpolated to the target initial crack lengths ($a = 3$ mm and 6 mm) by linear fits to the initial crack length a_{oq} for SE(T) J-resistance curves.

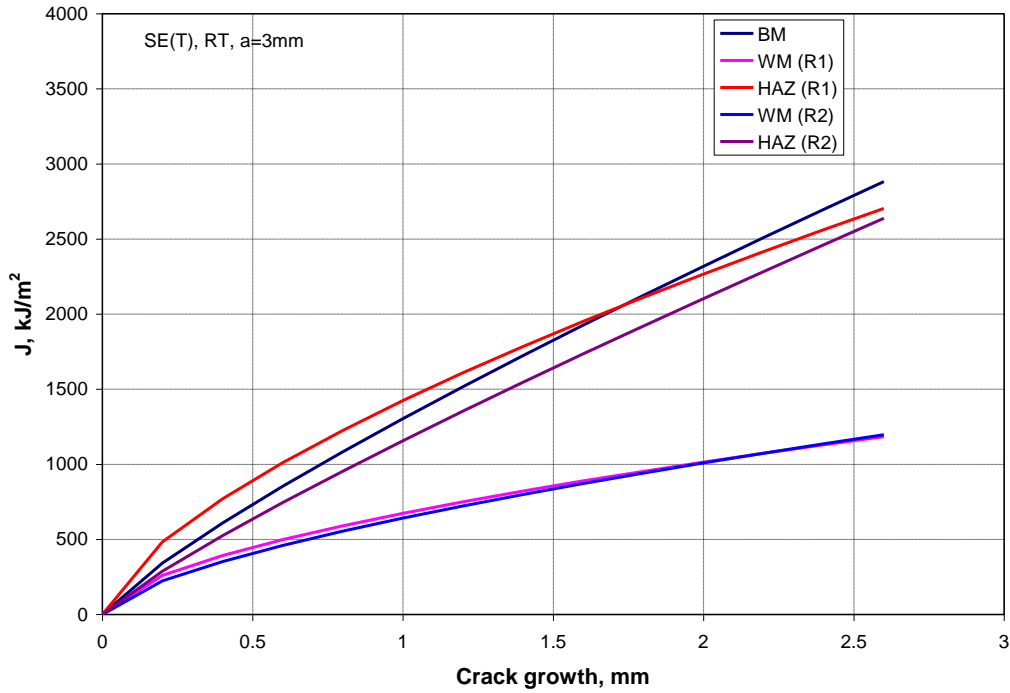
Target a_o (mm)	Temp. (°C)	Material	$C1$ (kJ/m ²)	$C2$	Remarks
3	RT	BM	1304	0.830	
		WM (R1)	674	0.590	
		HAZ (R1)	1424	0.671	
		WM (R2)	641	0.653	
		HAZ (R2)	1157	0.862	
	-20	BM	1500	0.857	
		WM (R1)	622	0.745	
		HAZ (R1)	1308	0.741	
		WM (R2)	505	0.886	
		HAZ (R2)	1147	0.821	
		WM (R3)	1164	0.656	$C1, C2$ averaged over 6 tests
	-40	HAZ (R3)	1555	0.537	$C1, C2$ averaged over 6 tests
		BM	*	*	
		WM (R1)	512	0.930	from an individual specimen ($a_{oq} = 3.3$ mm) - WMLT4K24
			616	0.740	from an individual specimen ($a_{oq} = 3.5$ mm) - WMLT4K25
		HAZ (R1)	1400	0.668	from an individual specimen ($a_{oq} = 3.6$ mm) - WMLT4K26
			1310	0.878	from an individual specimen ($a_{oq} = 2.6$ mm) - WMLT4K27
		WM (R2)	*	*	
HAZ (R2)	*	*			
6	RT	BM	1164	0.620	
		WM (R1)	564	0.710	
		HAZ (R1)	1132	0.560	
		WM (R2)	647	0.784	
		HAZ (R2)	948	0.604	
	-20	BM	1353	0.520	
		WM (R1)	505	0.763	
		HAZ (R1)	1006	0.712	
		WM (R2)	648	0.793	
		HAZ (R2)	985	0.830	

* no test data

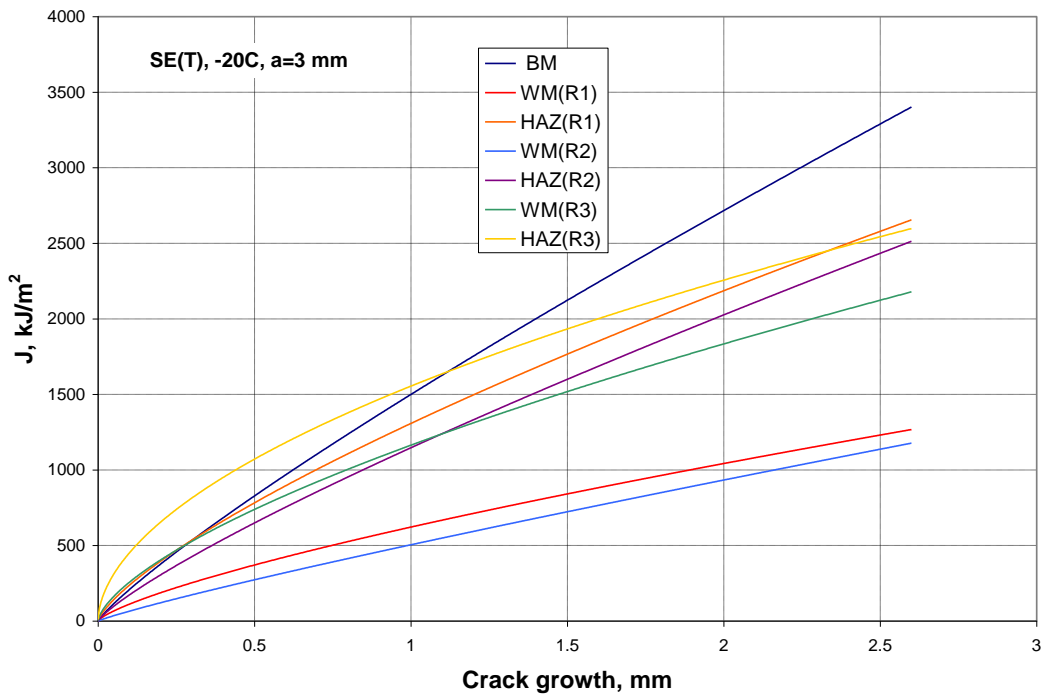
Table 13. Power-law fitting parameters $C1$ and $C2$ extrapolated/interpolated to the target initial crack lengths ($a = 3$ mm and 6 mm) by linear fits to the initial crack length a_{oq} for SE(B) J-resistance curves.

Target a_o (mm)	Temp. (°C)	Material	$C1$ (kJ/m ²)	$C2$	Remarks
3	RT	BM	*	*	
		WM (R1)	555	0.632	
		HAZ (R1)	979	0.685	
		WM (R2)	416	0.605	
		HAZ (R2)	*	*	
	-20	BM	1951	0.382	Round 3 – Pipe A $C1, C2$ averaged over 6 tests
		WM (R1)	486	0.532	
		HAZ (R1)	1208	0.691	
		WM (R2)	626	0.325	
		HAZ (R2)			
		WM (R3)	597	0.905	$C1, C2$ averaged over 6 tests
	HAZ (R3)	*	*		
6	RT	BM	1121	0.678	from an individual specimen ($a_{oq} = 5.4$ mm) - BBMRT1
			1124	0.729	from an individual specimen ($a_{oq} = 5.6$ mm) - BBMRT2
		WM (R1)	406	0.575	
		HAZ (R1)	936	0.712	
		WM (R2)	591	0.629	
		HAZ (R2)	*	*	
	-20	BM	*	*	
		WM (R1)	382	0.625	
		HAZ (R1)	979	0.760	
		WM (R2)	594	0.625	
HAZ (R2)	*	*			

* insufficient data

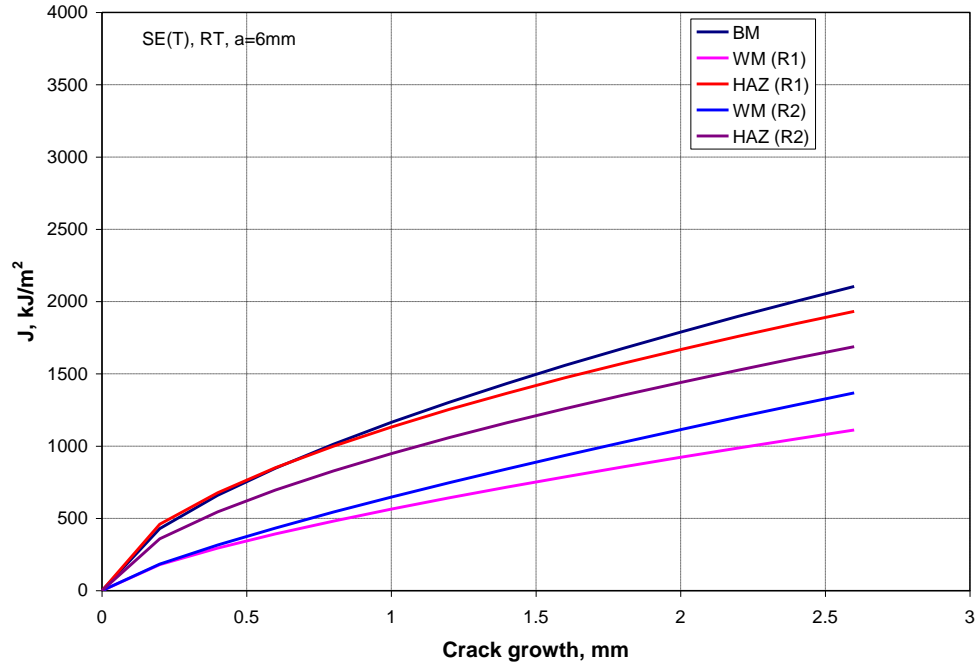


(a)

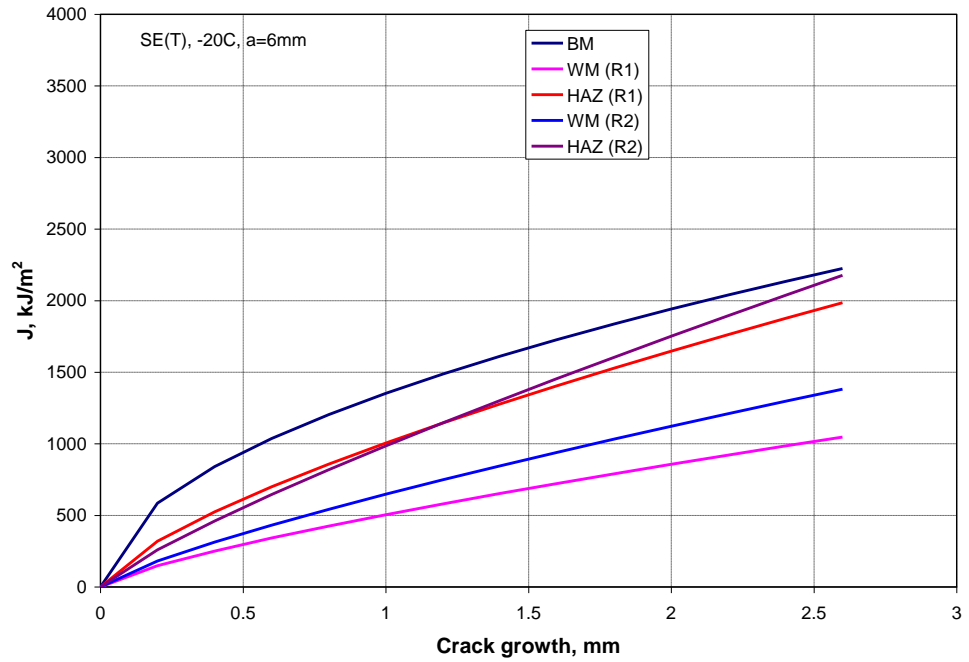


(b)

Figure 13. Cont'd.

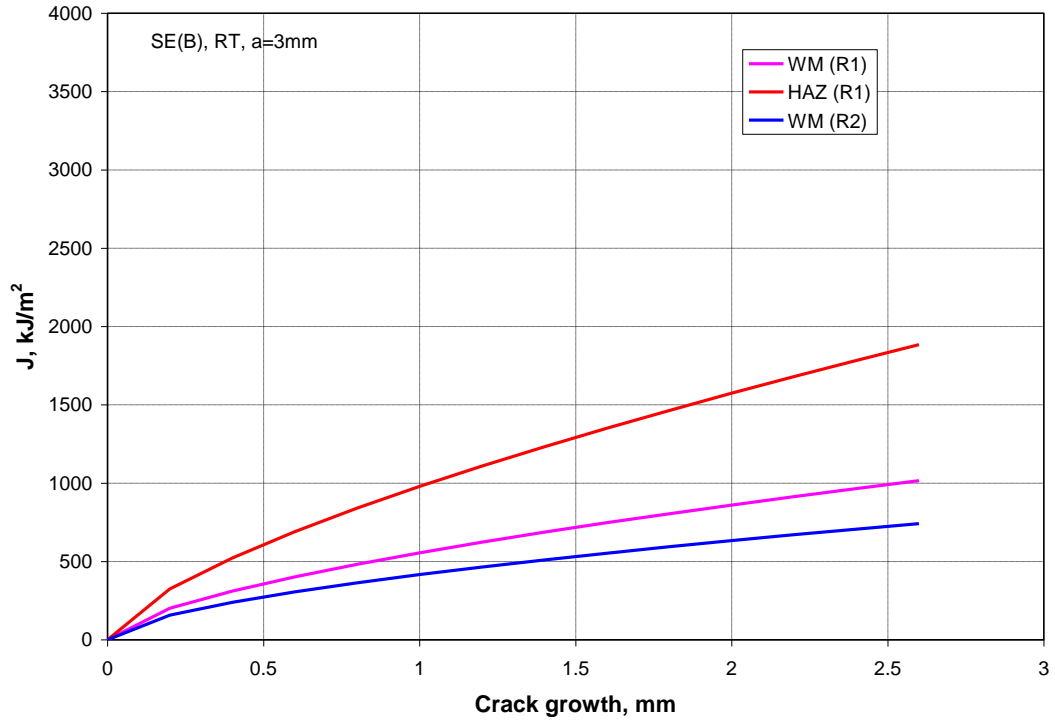


(c)

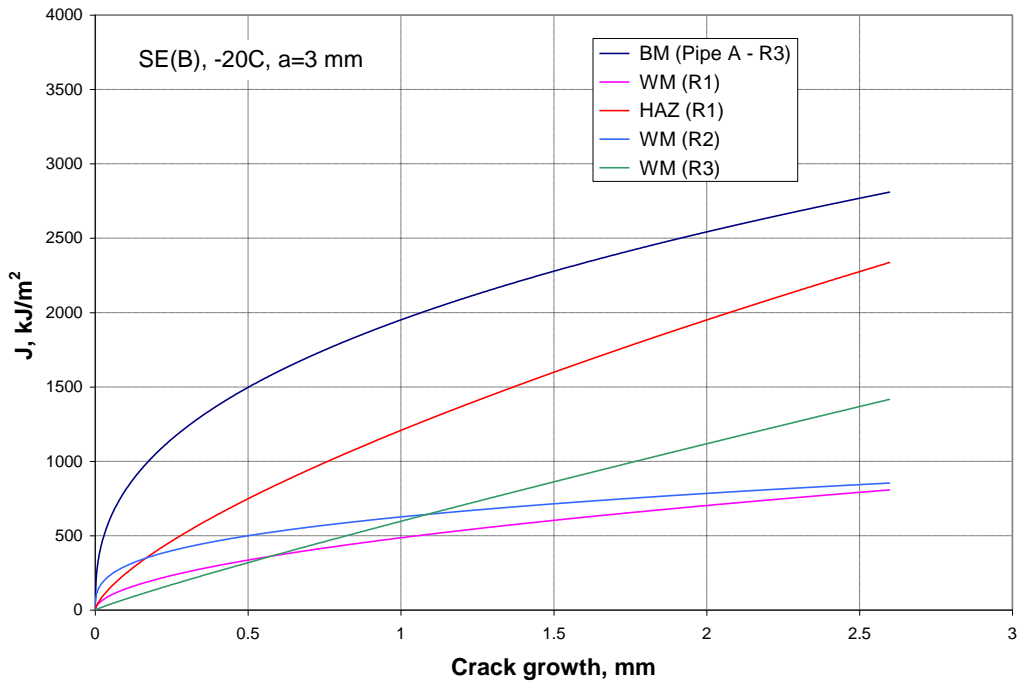


(d)

Figure 13. SE(T) J-resistance curves extrapolated/interpolated for the target crack lengths (3 mm and 6 mm), calculated with the $C1$ and $C2$ power-law parameters fit to a linear dependence on a/W or averaged: (a) RT, $a_o = 3$ mm, (b) -20 °C, $a_o = 3$ mm, (c) RT, $a_o = 6$ mm and (d) -20 °C, $a_o = 6$ mm. Owing to lack of data, fits of the parameters as a function of a/W were not obtained for base metal and HAZ (round 2).

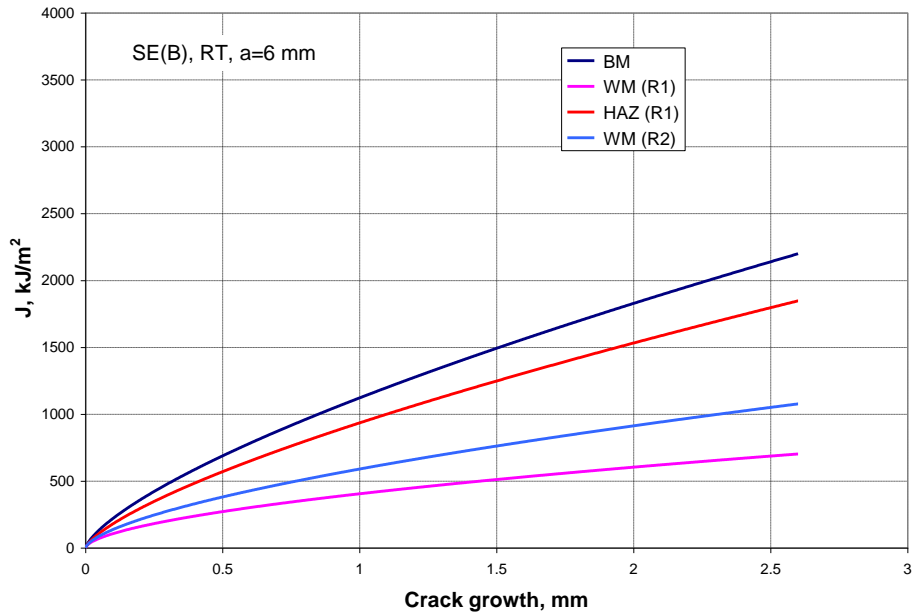


(a)

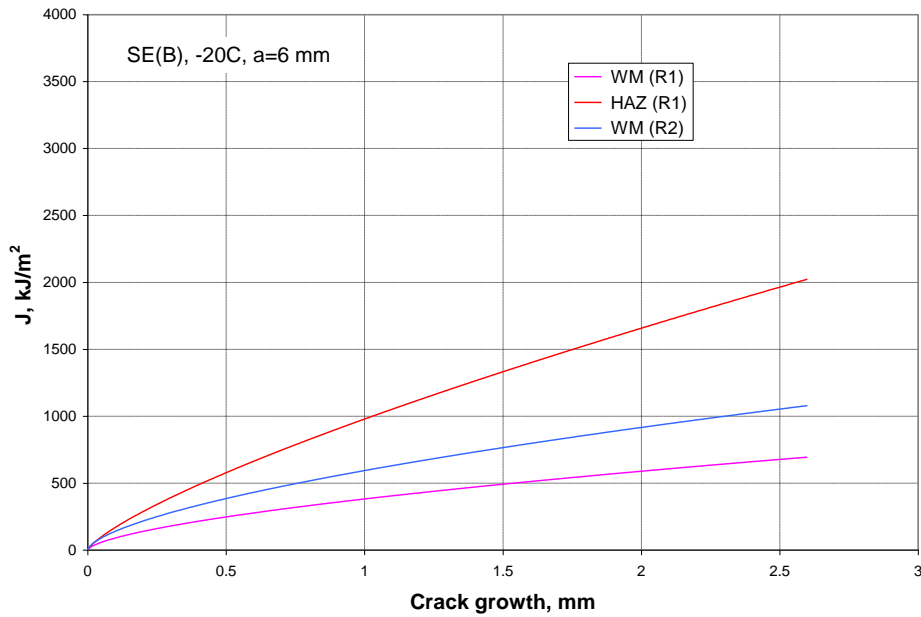


(b)

Figure 14. Cont'd.



(c)



(d)

Figure 14. SE(B) J-resistance curves extrapolated/interpolated for the target crack lengths (3 mm and 6 mm) calculated with the $C1$ and $C2$ power-law parameters fit to a linear dependence on a/W or averaged: (a) RT, $a_o = 3$ mm, (b) -20 °C, $a_o = 3$ mm, (c) RT, $a_o = 6$ mm and (d) -20 °C, $a_o = 6$ mm. Owing to lack of data, fits of the parameters as a function of a/W were not obtained for base metal (round 1 & round 2) and HAZ (round 2 and round 3).

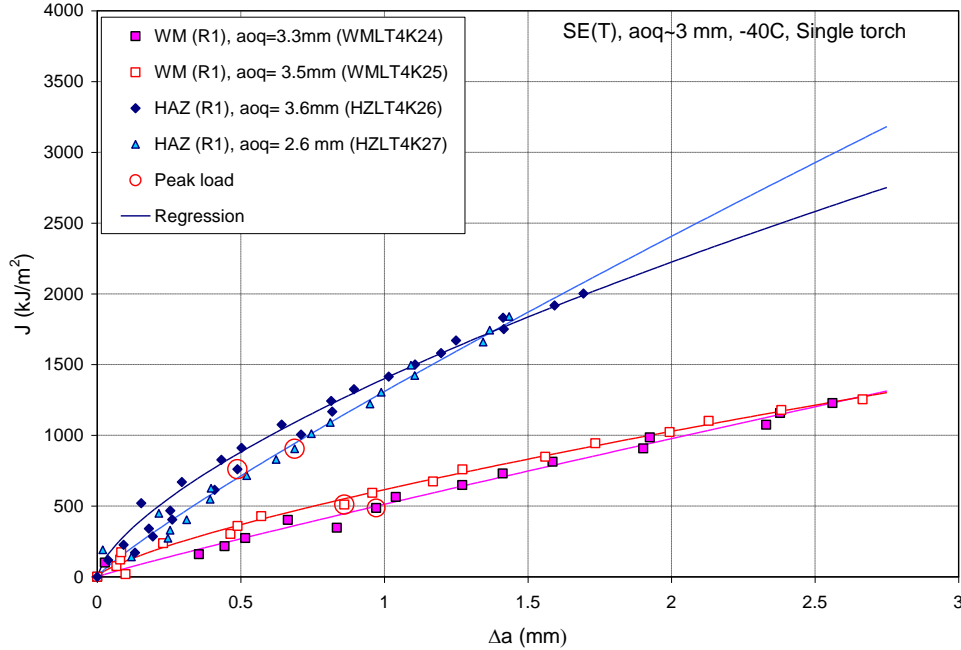


Figure 15. SE(T) J-resistance curves from experimental measurements of single-torch welds (WMC and HAZ regions) at test temperature of -40 °C (symbols: raw data, lines: fitting curves).

4.1.2 CTOD-Resistance Curves

Similarly to J-resistance curves, Table 14 and Table 15 summarize power-law fitting parameters $C1$ and $C2$ extrapolated/interpolated to the target initial crack lengths ($a = 3$ mm and 6 mm) by linear fits to the initial crack length (a_{oq}), for rounds 1 and 2 tests, or averaged (round 3), for SE(T) and SE(B) CTOD-resistance curves, respectively. Figure 16 and Figure 17 show CTOD-resistance curves, plotted with the $C1$ and $C2$ power-law parameters obtained as previously described. (For comparison, Figure 18 shows raw data and fitting curves for each crack length for SE(T) tests at -40 °C, for which linear fits of power-law fitting parameters to a/W are not available.) The general trends are similar to J-resistance curves seen in the previous section. The major difference is that the BM curve lies much higher than the HAZ and WM curves. This results from differences in yield strength. CTOD values here are converted from the corresponding J-values for SE(T) [2] and SE(B) [4], using the following relation:

$$CTOD = \frac{J}{m\sigma_Y}, \quad (3)$$

where m is a function of the work-hardening coefficient n and a/W and decreases for loads above the limit load as reported in 277-T-04; σ_Y is the effective yield strength. The WM overmatches the BM, which according to Eq. (3) causes the CTOD resistance curve for the WM to be depressed even further below that of the BM compared to their relative positions in the J-resistance curve. The yield strength of the WM is used in the conversion from J to CTOD for the HAZ, and so the HAZ CTOD resistance curves are lowered below the BM curves for the same reason as the WM curves.

Table 14. Power-law fitting parameters $C1$ and $C2$ extrapolated/interpolated to the target initial crack lengths ($a = 3$ mm and 6 mm) using linear fits to the initial crack length a_{oq} for SE(T) CTOD-resistance curves.

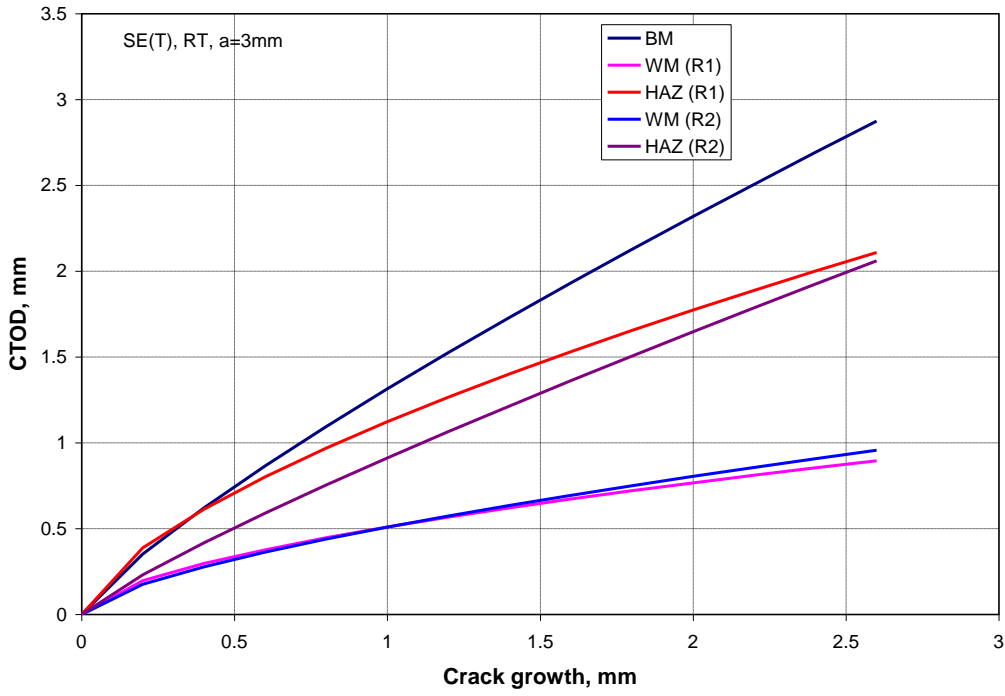
Target a_o (mm)	Temp. (°C)	Material	$C1$ (mm)	$C2$	Remarks
3	RT	BM	1.315	0.819	
		WM (R1)	0.510	0.590	
		HAZ (R1)	1.123	0.660	
		WM (R2)	0.509	0.661	
		HAZ (R2)	0.912	0.853	
	-20	BM	1.414	0.847	
		WM (R1)	0.460	0.756	
		HAZ (R1)	0.995	0.750	
		WM (R2)	0.372	0.912	
		HAZ (R2)	0.870	0.818	
		WM (R3)	0.797	0.681	$C1, C2$ averaged over 6 tests
	-40	HAZ (R3)	1.068	0.521	$C1, C2$ averaged over 6 tests
		BM	*	*	
		WM (R1)	0.361	0.960	from an individual specimen ($a_{oq} = 3.3$ mm) - WMLT4K24
			0.441	0.758	from an individual specimen ($a_{oq} = 3.5$ mm) - WMLT4K25
		HAZ (R1)	1.026	0.673	from an individual specimen ($a_{oq} = 3.6$ mm) - WMLT4K26
			0.971	0.904	from an individual specimen ($a_{oq} = 2.6$ mm) - WMLT4K27
		WM (R2)	*	*	
HAZ (R2)	*	*			
6	RT	BM	1.200	0.632	
		WM (R1)	0.434	0.756	
		HAZ (R1)	0.869	0.561	
		WM (R2)	0.492	0.822	
		HAZ (R2)	0.732	0.607	
	-20	BM	1.331	0.515	
		WM (R1)	0.356	0.823	
		HAZ (R1)	0.736	0.733	
		WM (R2)	0.476	0.826	
		HAZ (R2)	0.735	0.844	

* insufficient data

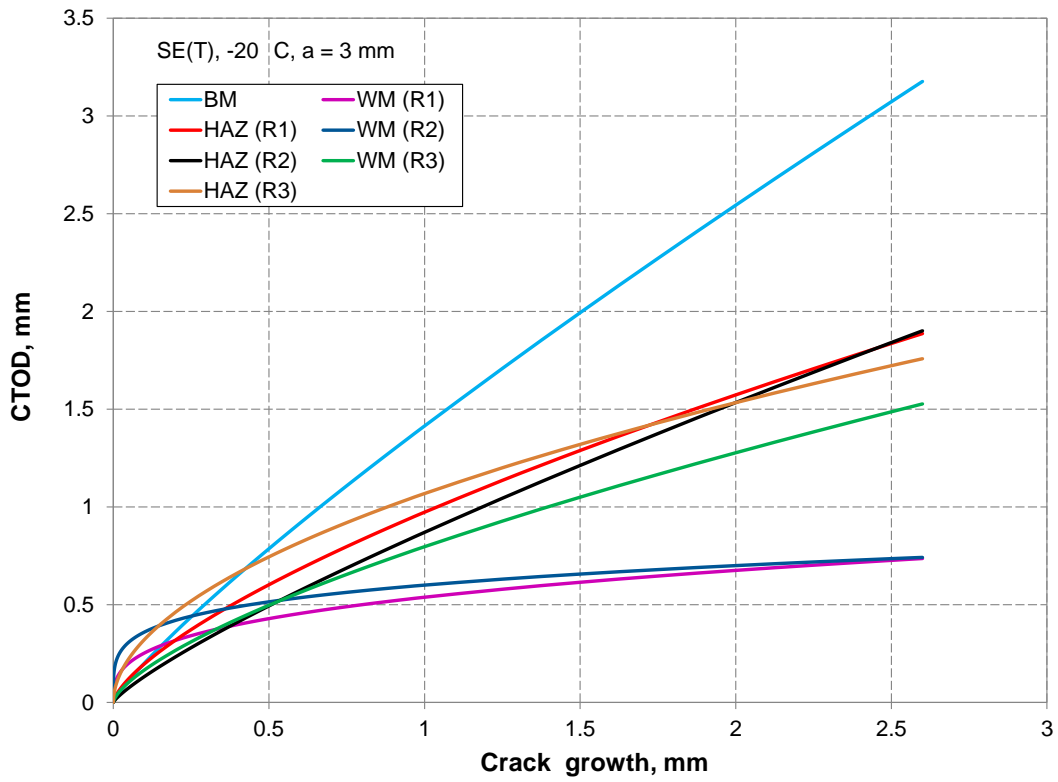
Table 15. Power-law fitting parameters $C1$ and $C2$ extrapolated/interpolated to the target initial crack lengths ($a = 3$ mm and 6 mm) by linear fits to the initial crack length a_{oq} for SE(B) CTOD-resistance curves.

Target a_o (mm)	Temp. (°C)	Material	$C1$ (mm)	$C2$	Remarks
3	RT	BM			
		WM (R1)	0.407	0.611	
		HAZ (R1)	0.720	0.659	
		WM (R2)	0.309	0.584	
		HAZ (R2)	*	*	
	-20	BM	1.220	0.678	Round 3 – Pipe A $C1, C2$ averaged over 6 tests
		WM (R1)	0.355	0.509	
		HAZ (R1)	0.891	0.673	
		WM (R2)	0.459	0.298	
		HAZ (R2)	*	*	
		WM (R3)	0.416	0.884	$C1, C2$ averaged over 6 tests
		HAZ (R3)	1.059	1.001	$C1, C2$ averaged over 3 tests
6	RT	BM	0.855	0.658	from an individual specimen ($a_{oq} = 5.4$ mm) - BBMRT1
			0.850	0.708	from an individual specimen ($a_{oq} = 5.6$ mm) - BBMRT2
		WM (R1)	0.280	0.556	
		HAZ (R1)	0.641	0.688	
		WM (R2)	0.404	0.606	
		HAZ (R2)	*	*	
	-20	BM	*	*	
		WM (R1)	0.261	0.605	
		HAZ (R1)	0.673	0.742	
		WM (R2)	0.406	0.603	
		HAZ (R2)	*	*	

* insufficient data

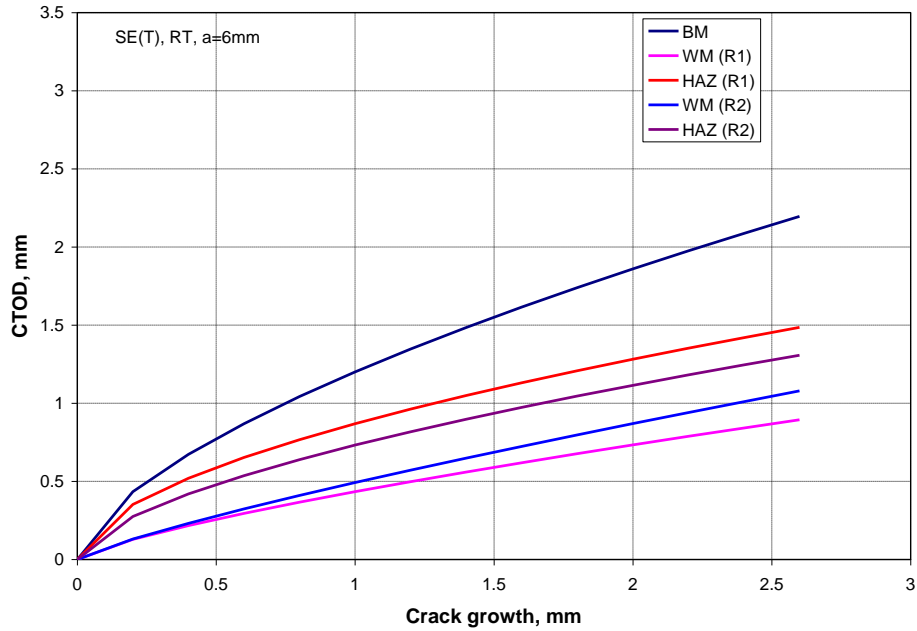


(a)

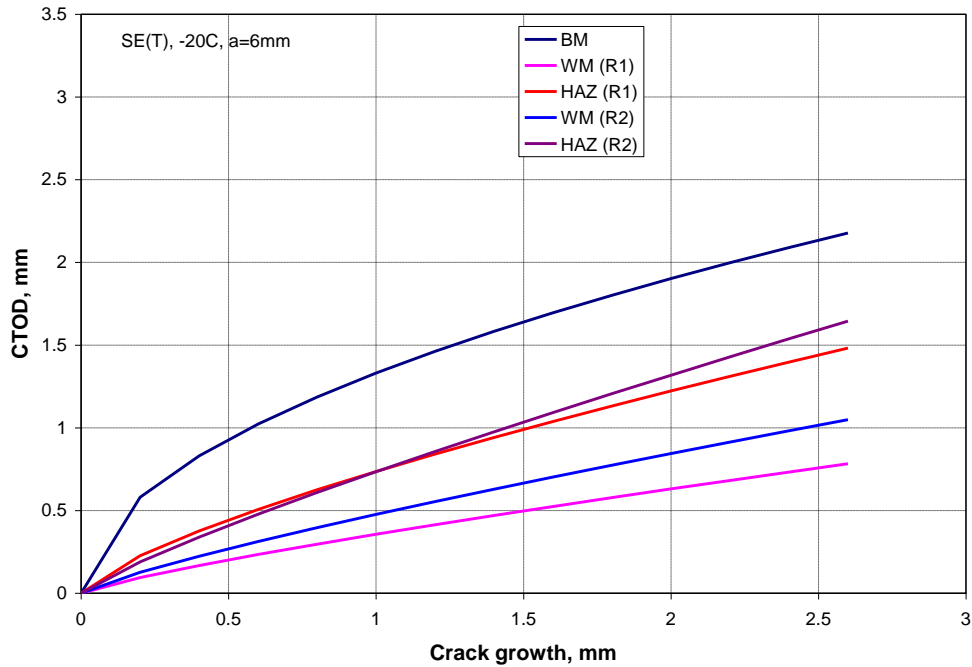


(b)

Figure 16. Cont'd.

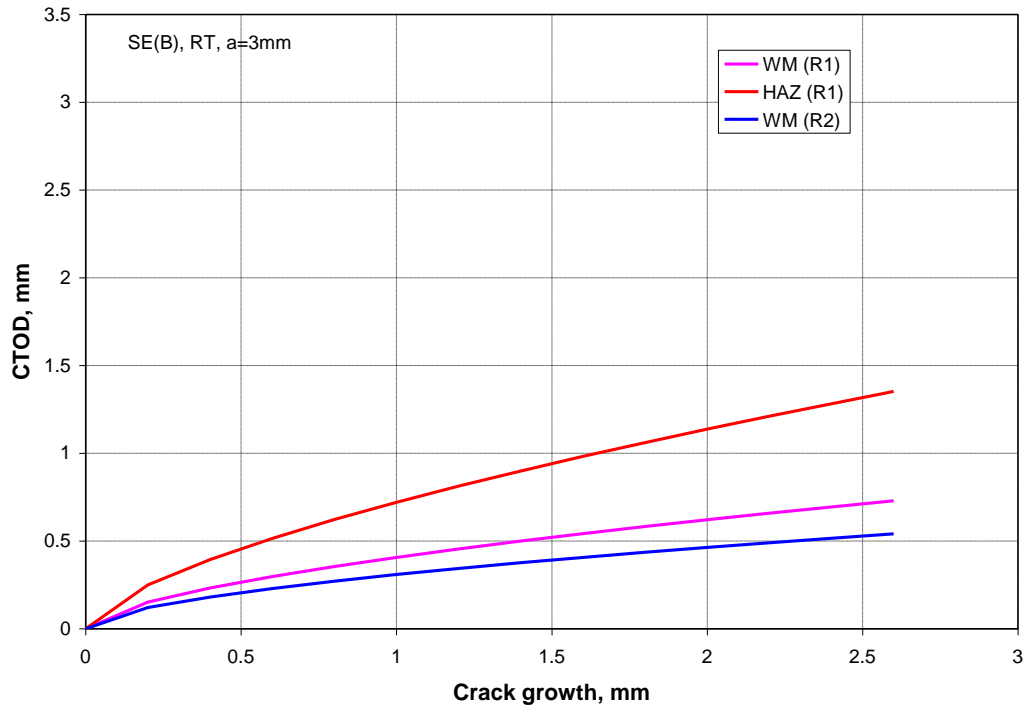


(c)

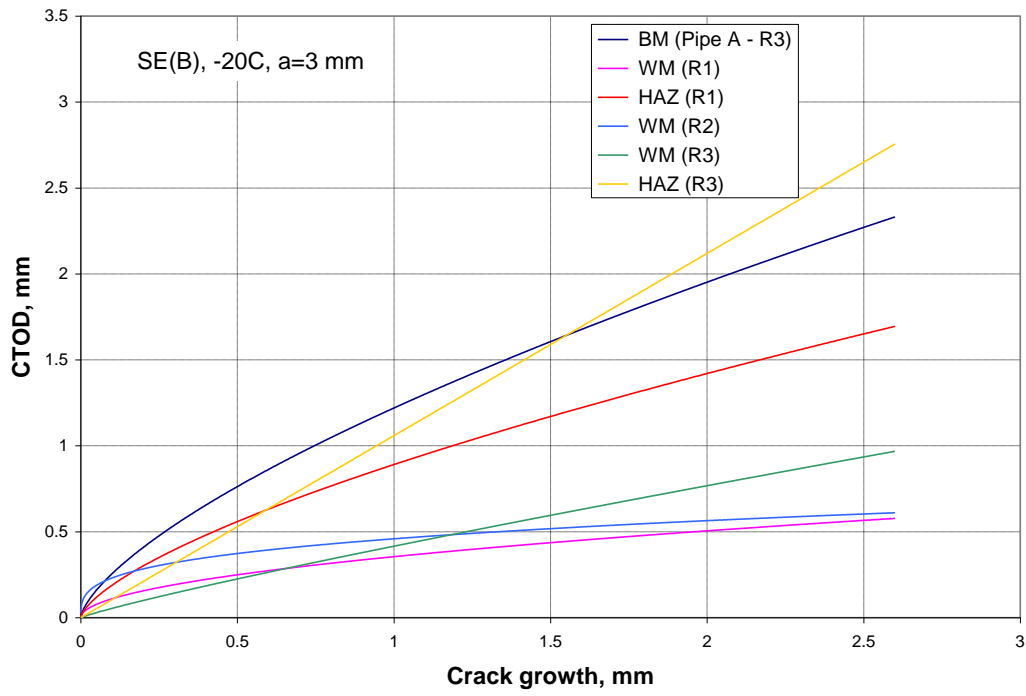


(d)

Figure 16. SE(T) CTOD-resistance curves extrapolated/interpolated for the target crack lengths (3 mm and 6 mm) with the $C1$ and $C2$ power-law parameters fit to a linear dependence on a/W or averaged: (a) RT, $a_o = 3$ mm, (b) -20 °C, $a_o = 3$ mm, (c) RT, $a_o = 6$ mm and (d) -20 °C, $a_o = 6$ mm. Owing to lack of data, fits of the parameters as a function of a/W were not obtained for base metal and HAZ (round 2).

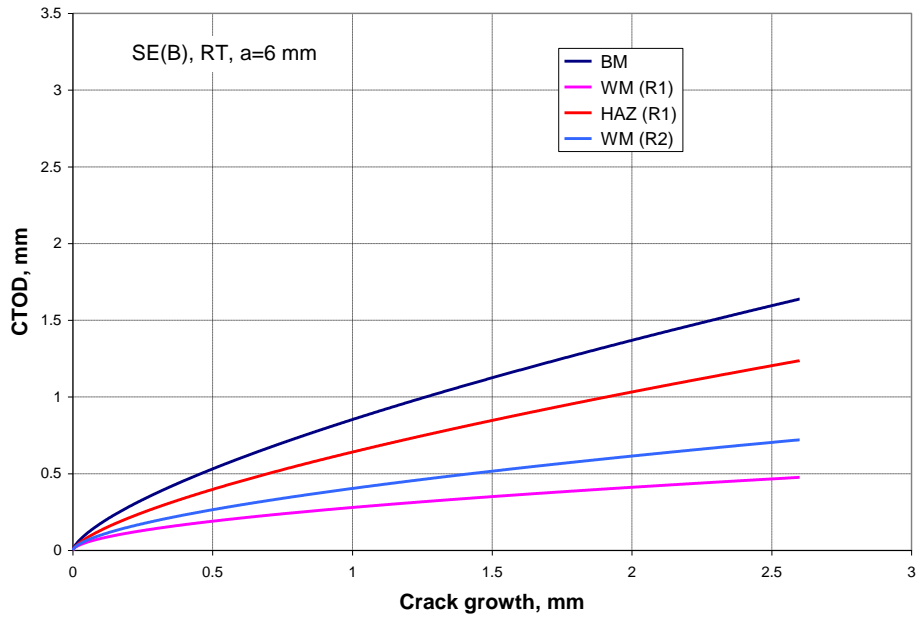


(a)

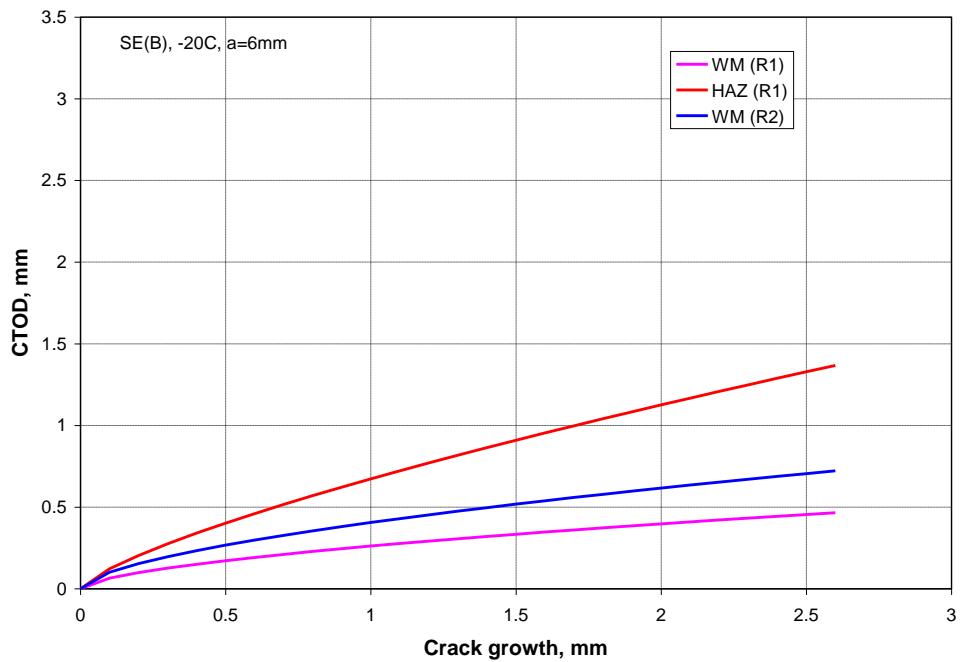


(b)

Figure 17. Cont'd.



(c)



(d)

Figure 17. SE(B) CTOD-resistance curves extrapolated/interpolated for the target crack lengths (3 mm and 6 mm) with the $C1$ and $C2$ power-law parameters fit to a linear dependence on a/W or averaged: (a) RT, $a_o = 3$ mm, (b) -20 °C, $a_o = 3$ mm, (c) RT, $a_o = 6$ mm and (d) -20 °C, $a_o = 6$ mm. Owing to lack of data, fits of the parameters as a function of a/W were not obtained for base metal (round 1 & round 2) and HAZ (round 2).

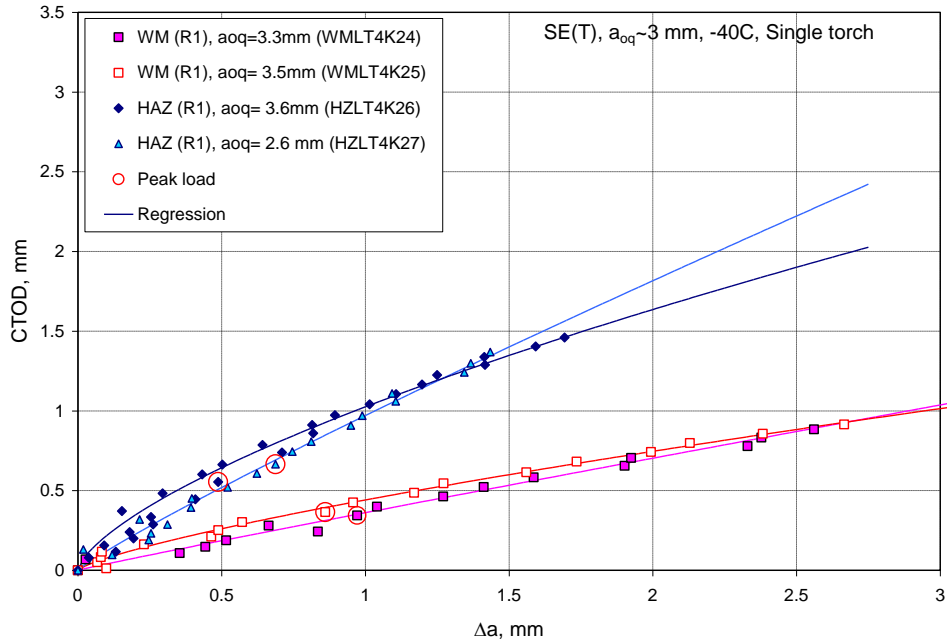


Figure 18. SE(T) CTOD-resistance curves from experimental measurements of single-torch welds (WMC and HAZ regions) at test temperature of -40 °C.

4.1.3 Brittle Fracture

Brittle fractures were observed for some of the HAZ specimens tested at -20 °C. Table 16 summarizes statistics of the brittle fractures observed in this study. Fracture surfaces and resistance curves are shown in the separate report [5]. Note that all other SE(T) and SE(B) specimens tested in this study were fully ductile, including SE(T) specimens tested at -40 °C; refer to Table 4 through Table 11 for the number of other tested specimens.

Table 16. Statistics of brittle fracture at -20 °C.

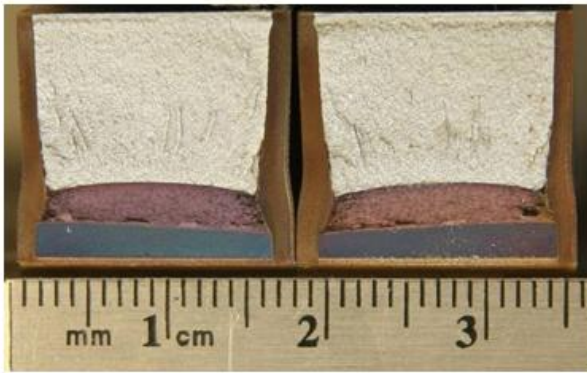
Loading Mode	Material	Test temp. (°C)	Target crack length, a (mm)	Total no. of tested specimens	Brittle fracture	
					Before peak load	After peak load
SE(T)	HAZ (R1)	-40	3	2	0	0
		-20	3	3	1	1
	6		3	0	0	
	HAZ (R2)		3	2	0	0
	6		2	0	0	
	HAZ (R3)	3	6	0	1	
SE(B)	HAZ (R1)	-20	3	2	1	1 (pop-in)
			6	2	0	2
	HAZ (R2)		3	1	0	1
	6		1	0	1	
	HAZ (R3)		3	5	1	4 (2 pop-ins)

As expected, brittle fractures or pop-ins are more frequent in SE(B) than in SE(T) specimens (three brittle fractures out of eighteen SE(T) specimens and eleven out of eleven SE(B) specimens), because the higher constraint in the former geometry generates higher triaxial stress at the crack tip, which promotes cleavage. It was observed that brittle fracture was more common in specimens notched in the HAZ, especially for $a_o = 3$ mm. This may be attributed to the microstructure sampled at the crack tip. As seen in Figure 2(b), the geometry of weld metal and the location of the initial fatigue crack for $a_o = 3$ mm can easily lead to crack growth from the HAZ region to the fusion line and weld metal. In this case, cleavage can be triggered when the crack reaches a brittle microstructure, which is often found in the vicinity of the fusion line. Observations indicate that the crack tends to grow toward lower-strength material, and so the softer HAZ would tend to focus the crack toward the fusion line.

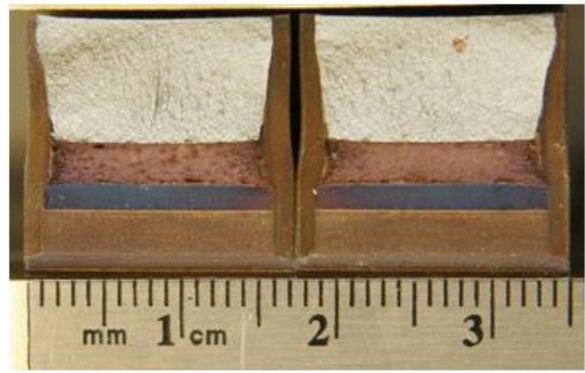
4.2 Post-test Analysis

4.2.1 Side Grooving

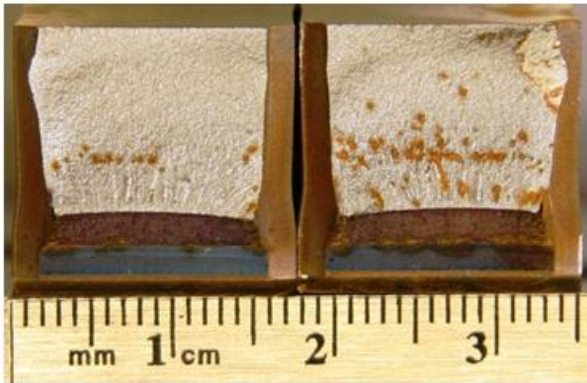
Based on previous studies [8,9], all SE(T) and SE(B) specimens from rounds 1 and 2 were side grooved by 7.5 % of thickness (B) on each side after fatigue precracking, in order to provide a condition along the crack front as close as possible to plane strain and, consequently, to achieve a straight crack front. SE(T) and SE(B) specimens from round 3, however, were side grooved by 5 % of B on each side, for a total thickness reduction of 10 % (with the exception of one WM specimen, designated DW1-B, that was tested in plane-sided condition). Optical observations of fracture surfaces (Figure 19) verify that specimens with 15 % side grooves (7.5 % on each side) show relatively straight crack fronts, while a specimen with 20 % side-grooves (10 % on each side) and $a_o \approx 6$ mm exhibits a concave crack front for the deeper crack. The same is shown in Figure 20, for SE(B) base metal specimens from round 3 with 10 % side-grooving (5 % per side), for which the crack front is convex, especially near the edges. The results suggest that 15 % B side grooving (7.5 % on each side) is optimal, at least for this material; almost all specimens with this SG depth satisfy the final crack size and crack extension requirements of the BS and ASTM standards. As shown in Figure 21(round 3 WM specimens), 10 % side grooving has only a small effect on the resistance curve compared with a plane-sided sample. This implies that 10 % side-grooving is insufficient to establish plane strain conditions across the crack front, because it is known from previous work that constraint is significantly higher and R curves lower in specimens side-grooved by 15 and 20 % compared with plane-sided specimens (see section 4.3). SE(T) specimens are particularly sensitive to the depth of side-grooving because of the shallow stress gradient in the crack growth direction compared with SE(B) specimens.



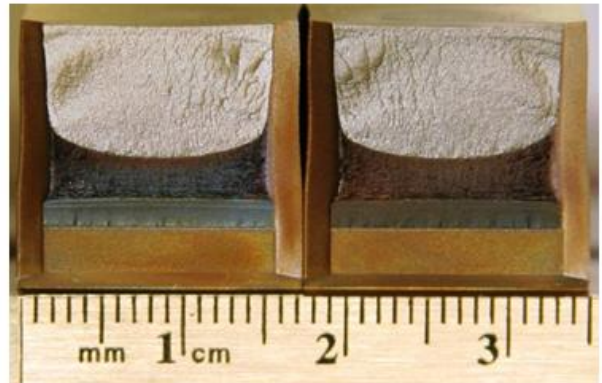
(a) $a_0 \sim 3\text{mm}$ (15% SG)



(b) $a_0 \sim 6\text{mm}$ (15% SG)



(c) $a_0 \sim 3\text{mm}$ (20% SG)



(d) $a_0 \sim 6\text{mm}$ (20% SG)

Figure 19. Representative fracture surfaces of SE(T) base metal specimens from rounds 1 and 2 (side grooving: 15 % and 20 %).

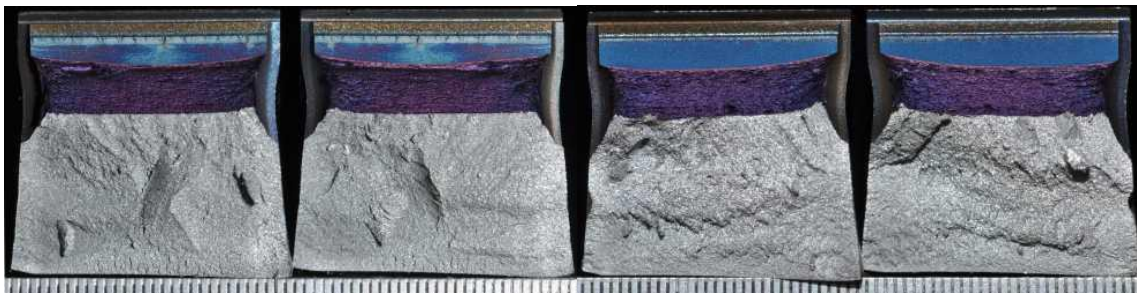


Figure 20. Representative fracture surfaces of SE(B) base metal specimens from round 3 (side grooving: 10 %). Scale graduations equal 0.5 mm.

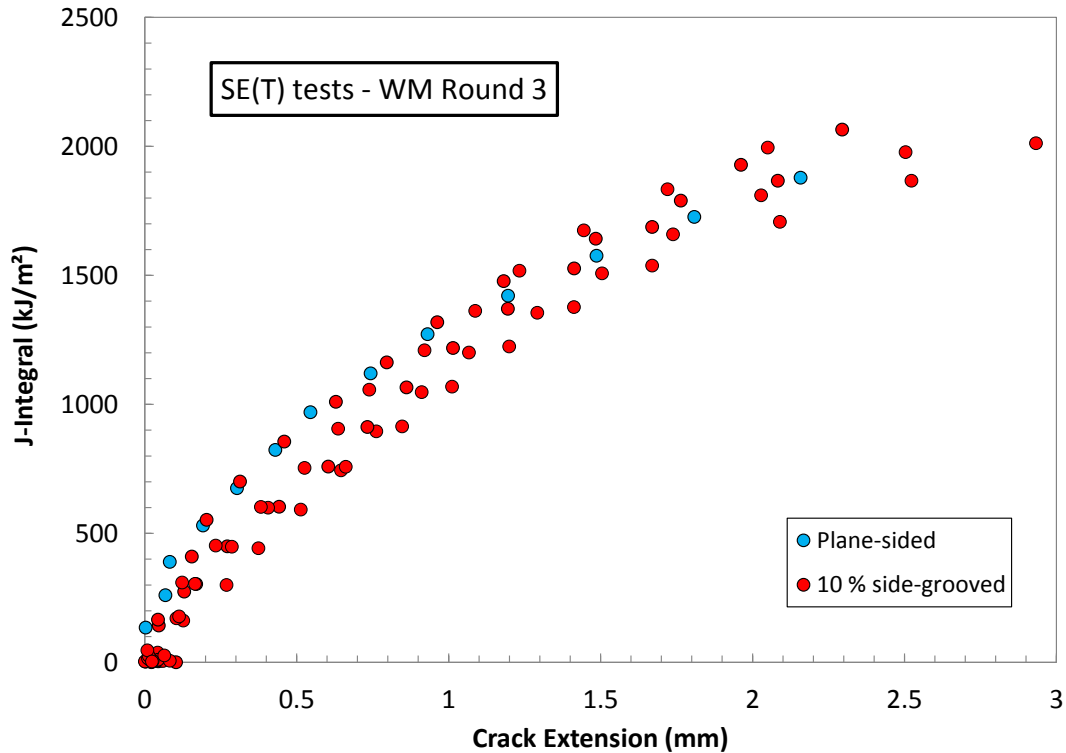


Figure 21. Comparison between plane-sided (1 specimen) and 10 % side-grooved (5 specimens) SE(T) test results for WM (round 3).

4.2.2 Crack Length Measurements

The unloading-compliance-predicted crack lengths agree well with optical measurements for the BM, WM and HAZ specimens as reported separately [5]. Measured crack lengths also meet the crack size requirements of the BS and ASTM standards for the majority of tested specimens (Table 2 and Table 3), particularly for R1 and R2 tests, on account of the beneficial effect of 15 % side-grooving. Success in meeting the requirements of the standards was significantly higher in R1 and R2 tests compared with R3 (Table 1 and Table 3), supporting the argument above that 10 % side-grooving is not quite sufficient to generate plane-strain conditions. For HAZ specimens, the overmatching strength of the weld metal results in asymmetrical deformation at the crack tip, which leads to biased crack growth and different apparent crack lengths on the base metal and weld metal sides. Some crack lengths measured on the BM side do not fulfill the standard crack size requirements. This will be discussed in detail in Section 2.2.

4.3 SE(T) Test Comparison: Single- vs. Multi-specimen

As a comparison activity, TWI Ltd. (U.K.) carried out tests with a SE(T) multi-specimen technique according to DNV RP F108 [11]. Figure 22 compares J-resistance curves from the SE(T) clamped single-specimen CANMET technique and the multi-specimen technique for $a_0 \approx 6$ mm at room temperature. Note that the specimens for the multi-specimen test were plane-sided, while the single-specimen method applied 15 % side grooving as described earlier. For J-value calculation, in the multi-specimen method there is no correction for crack growth, but there is

such a correction in the CANMET method, with the use of a/W -dependent parameters η and γ [12]. For compatible comparison, J values of one of the specimens from the single-specimen CANMET tests were calculated without crack growth correction, *i.e.*, γ was set to zero, and the value of η was not changed (*i.e.*, taken as the initial value) as the crack grew; results are shown in Figure 22. Removal of the crack growth correction does not make a large difference, but nevertheless the CANMET and TWI results are in close agreement. This agreement is somewhat fortuitous, resulting from compensating effects of a conservative factor in the DNV method and the use of side grooves in the CANMET procedure. RP F108 applies a factor of 0.85 to the J calculation to give a conservative resistance curve. The CANMET procedure calls for side grooves, and it is known from CANMET experience [8] that for $B \times B$ specimens, the introduction of 20 % side grooves leads typically to a 30 % reduction of the resistance curve in both SE(T) and SE(B) tests. This suggests that the absence of side grooves in the $B \times 2B$ specimens tested by TWI could raise the resistance curve significantly. The lower constraint at the surface of the plane-sided specimens tested by TWI is supported by the observation that the crack growth is much smaller at the surface than at the centre of these specimens, with the surface growth being typically only about 50 % of the growth at the centre. It is thus reasonable to conclude that in the TWI tests a reduction of the resistance curve from the 85 % “conservative” factor is balanced by an elevation of the curve owing to the absence of side grooves.

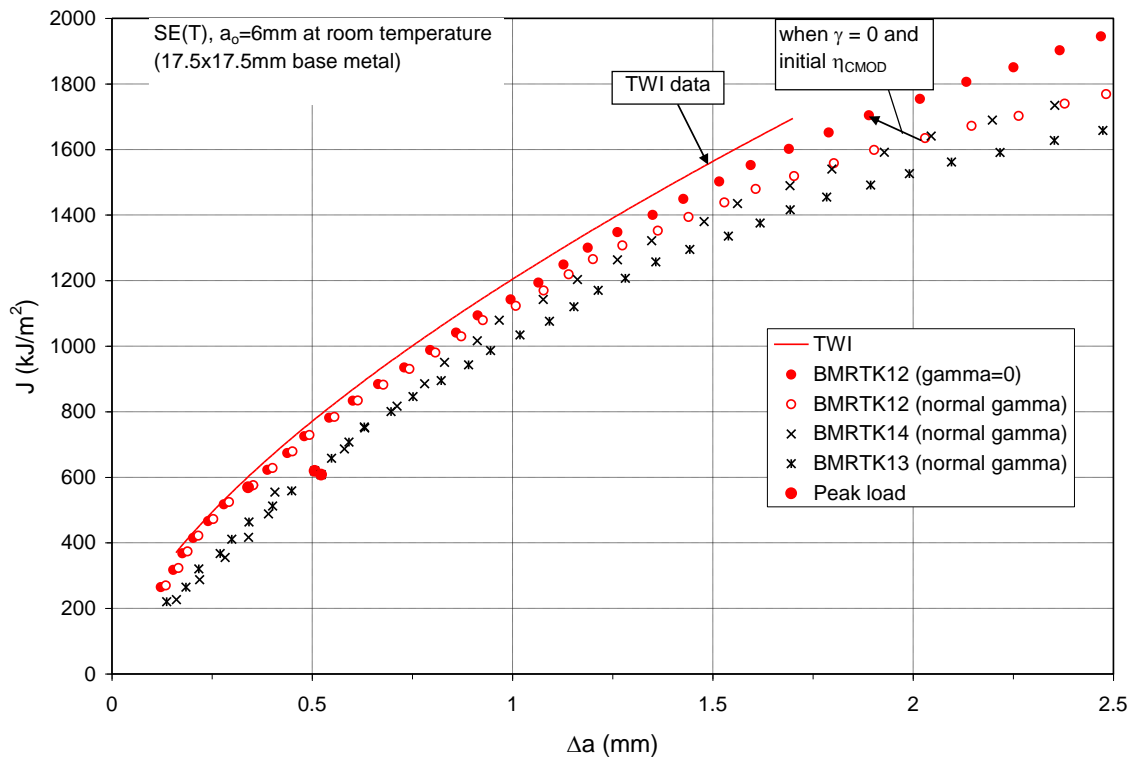
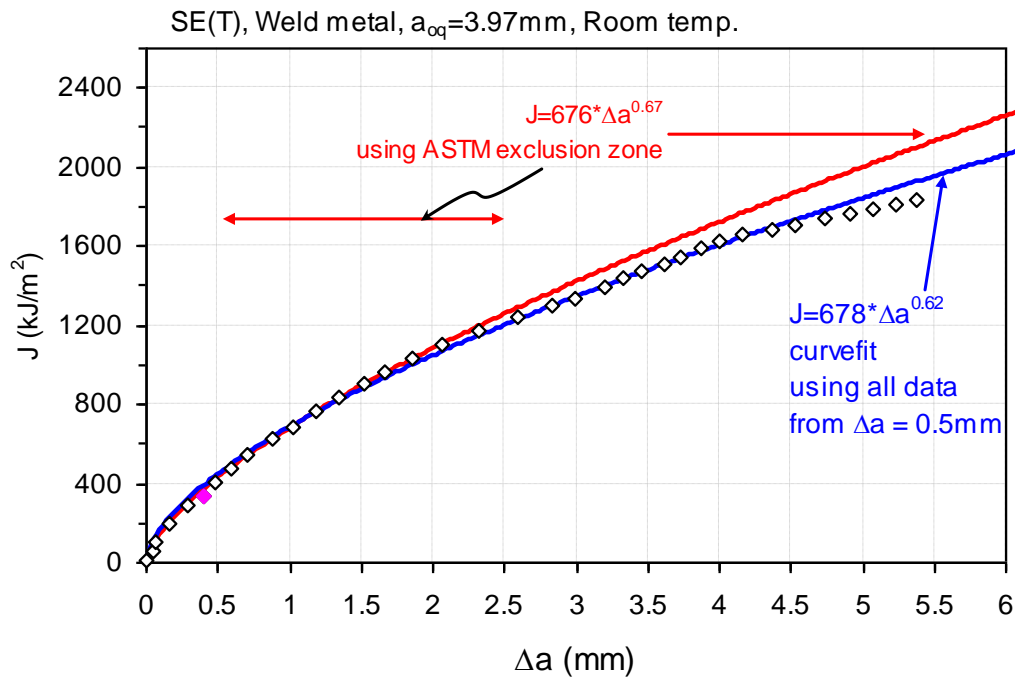


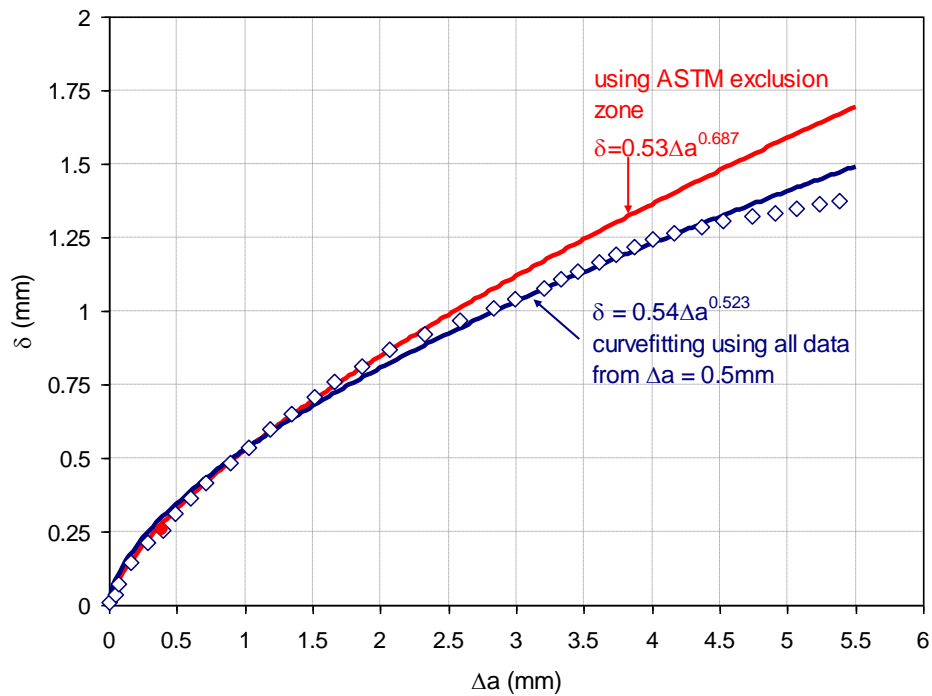
Figure 22. Comparisons of J-resistance curves from SE(T) multi-specimen and single-specimen techniques.

4.4 Validation of Power-law Regression

As discussed earlier, J- and CTOD-resistance data were curve-fit to power-law regressions according to the procedure of ASTM E1820-11 [4] for both SE(T) and SE(B) tests. The ASTM procedure uses $J-\Delta a$ data points that fall inside the area enclosed by the 0.15 mm and 1.5 mm exclusion lines, where exclusion lines are drawn parallel to the blunting line intersecting the abscissa at 0.15 mm and 1.5 mm. The fitted resistance curves are to be used for comparison with curved-wide-plate (CWP) test measurements of the actual crack length performed at NIST for development of a strain-based design procedure. The CWP results indicate that the instability (strain) occurs at a crack growth of a several millimeters. For instability analysis, it is required to have resistance curves that extend beyond the expected instability point. Hence, one specimen was tested well beyond the usual range of crack growth (to more than 5 mm crack growth, *i.e.* for growth through nearly half the ligament), for comparison of regression curves from data below 1.5 mm with experimental data measured well beyond this value. The difference between the curves is generally less than 10 % (Figure 23). Note that all regression curves of resistance plots in this study are generated according to the ASTM procedure, *i.e.*, with the use of data between the 0.15 mm and 1.5 mm exclusion lines, rather than with all collected data. Note also that the specimen measuring capacity, both in terms of J (J_{limit}) and CTOD (δ_{limit}), has not been used as an upper validity limit as prescribed by ASTM E1820-11. This is consistent with the approach taken in this project that geometry-dependent R curves are relevant to prediction of CWP behaviour provided the geometry (a/W and W) is the same as that in the CWP tests. In other words, the R curves generated in this work are not material properties in the sense of being independent of specimen size, but they are precisely the curves that are appropriate for ECA.



(a)



(b)

Figure 23. Comparisons of regression methods with measurements for single-torch weld metal centerline specimens ($a_o = 4$ mm): (a) J-resistance curve and (b) CTOD-resistance curve (Symbols: calculations from unloading compliance measurements; solid lines: regressions). The solid symbol (near $\delta = 0.25$ mm) corresponds to the maximum force attained during the test.

4.5 Effects of Material, Constraint and Temperature

J- and CTOD-resistance curves of WM (both single- and dual-torch) are much lower than those of BM and HAZ, regardless of initial crack length (Figure 13-18). This is attributed to the effect of weld microstructure, which can make the toughness of WM lower [13]. Figure 24(b) and (d) show numerous large voids near the crack tip in WM but relatively fewer voids in the HAZ; large voids are marked by “V” in the figures. Close observation also reveals a higher content of microvoids in the weld. The voids could be a result of micro-porosity in the WM or from growth of voids from inclusions in the fracture process zone. Another observation is that the crack-tip opening angle (CTOA) in the WM is much smaller than in the HAZ. This suggests a low crack propagation resistance of the WM, which in turn results in a low slope of the resistance curve as seen in Figure 13-18. It is well known that a high density of inclusions reduces ductile toughness, because inclusions nucleate voids which play a key role in crack growth. The lower toughness of the WM is understandable in terms of the higher density of void-forming sites (e.g. inclusions) than in the HAZ or BM.

Figure 25-28 compare J and CTOD values as a function of initial crack length at $\Delta a = 0.5$ mm and 2 mm for SE(T) and SE(B) tests of BM, WM and HAZ specimens. Although significant scatter is observed at $\Delta a = 0.5$ mm, the results show that toughness generally increases with decreasing initial crack length for all materials as anticipated, owing to the

dependence of constraint on initial crack length (higher constraint for deeper cracks). The dual-torch WM (round 2), however, is relatively insensitive to initial crack length. Toughness is sensitive to microstructure, and the higher density of inclusions in the WM may influence this observed insensitivity to constraint.

Test temperature did not significantly affect toughness of the base metal, HAZ or weld metal. J and CTOD values at room and $-20\text{ }^{\circ}\text{C}$ lie within a scatter band, which can be considered typical of material variability for a given region.

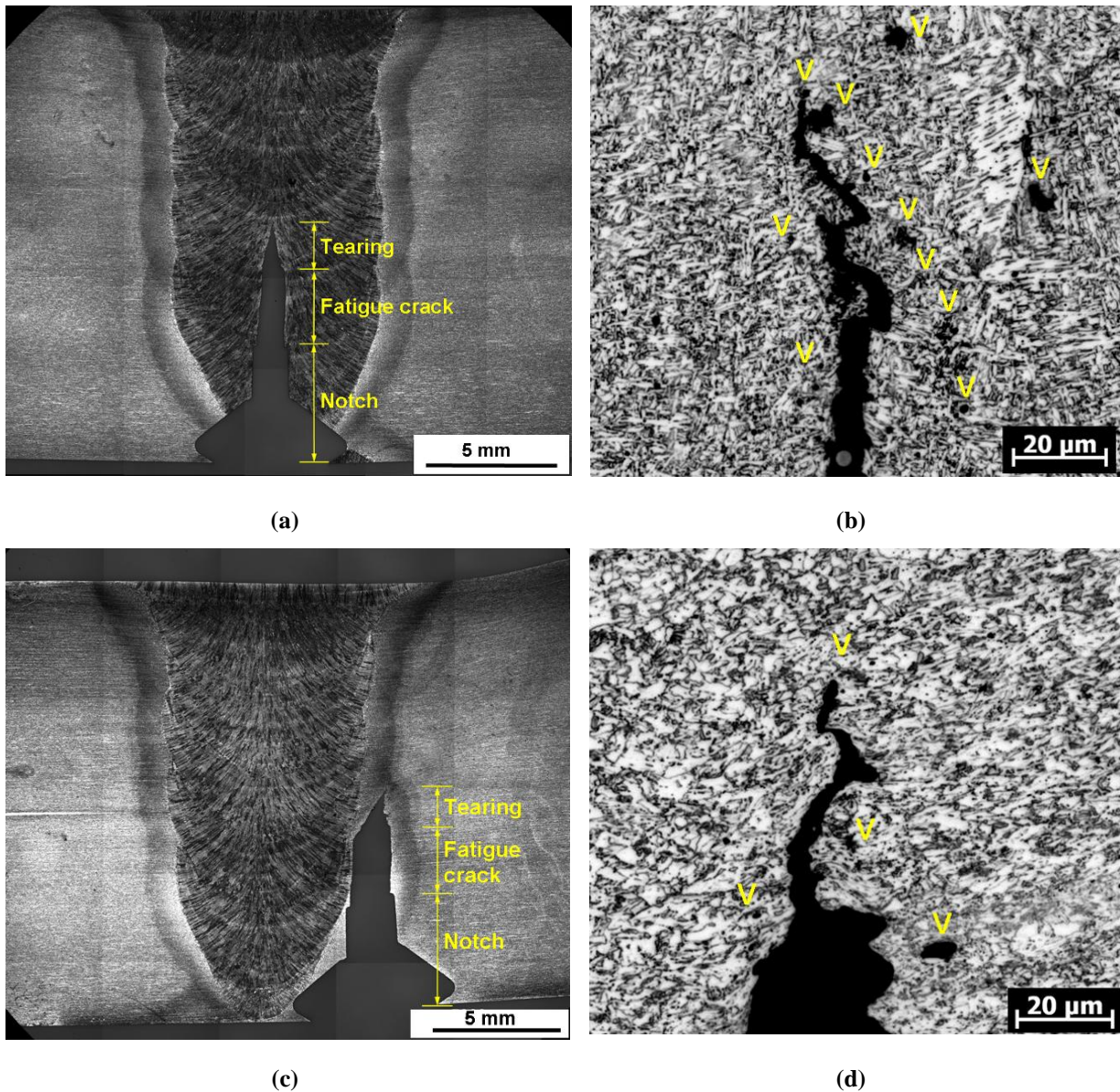
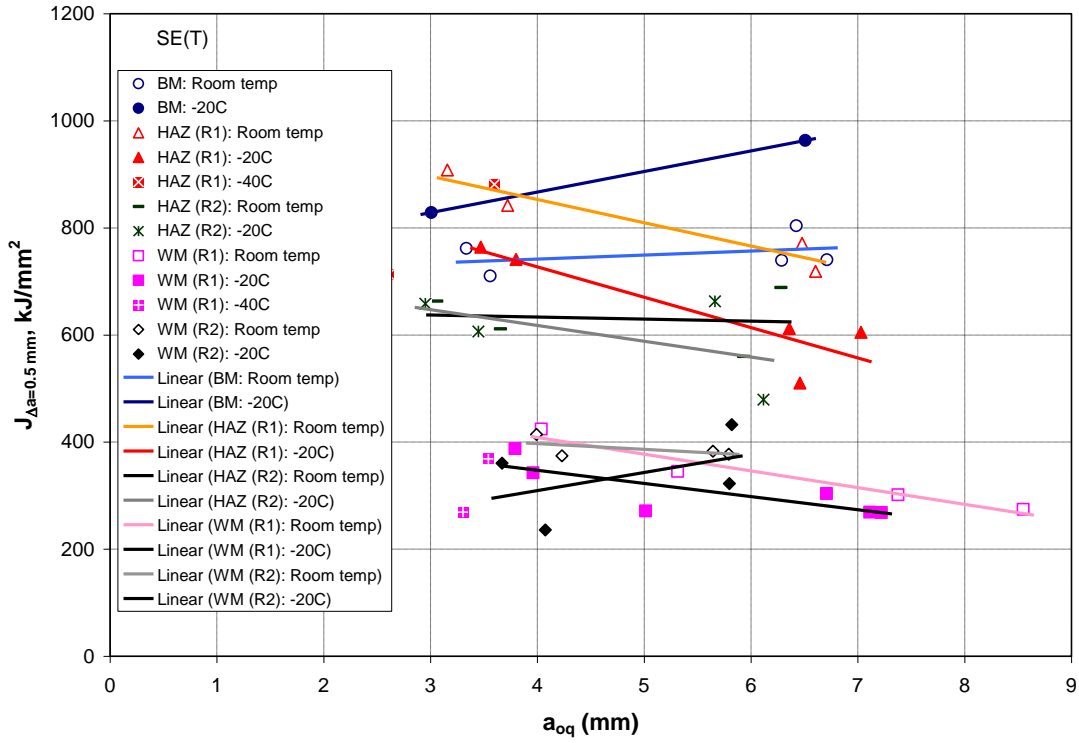
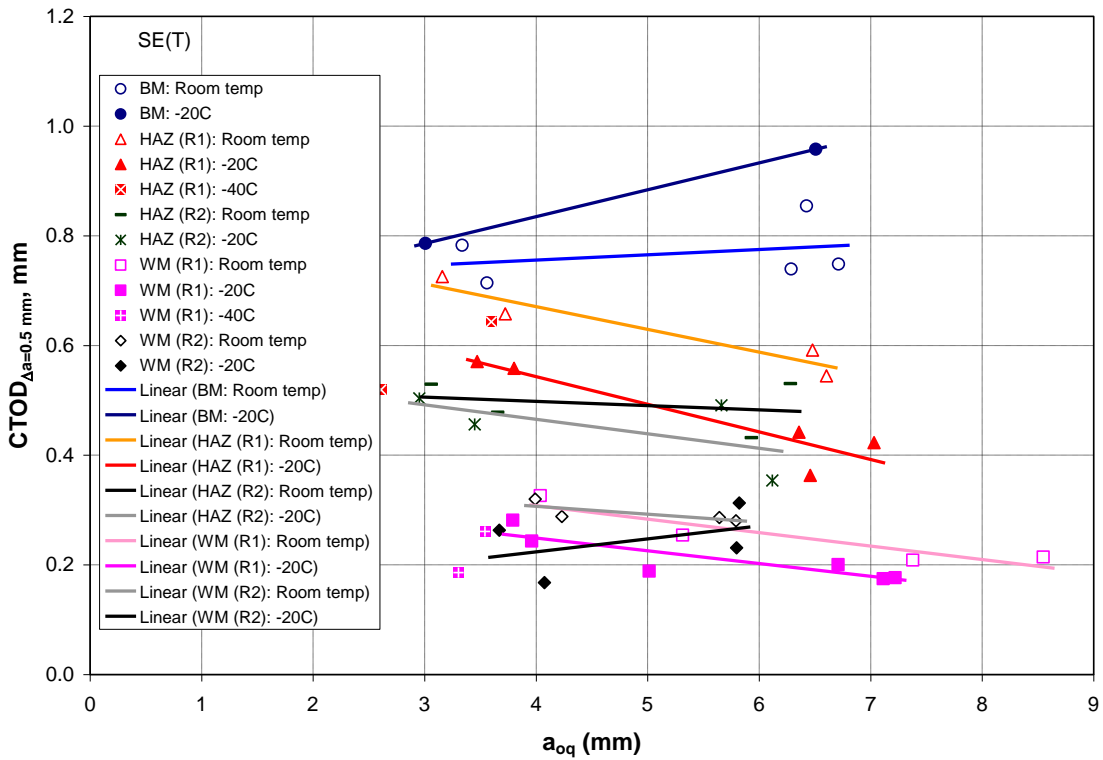


Figure 24. Optical microscope images of etched mid-thickness sections of SE(T) specimens: weld metal centerline specimen (WMLTK14) [(a) and (b)] and HAZ specimen (HZLTK17) [(c) and (d)], (b) and (d) show enlarged images near the crack tip of (a) and (c), respectively, and large voids are marked by “V” in the figures.

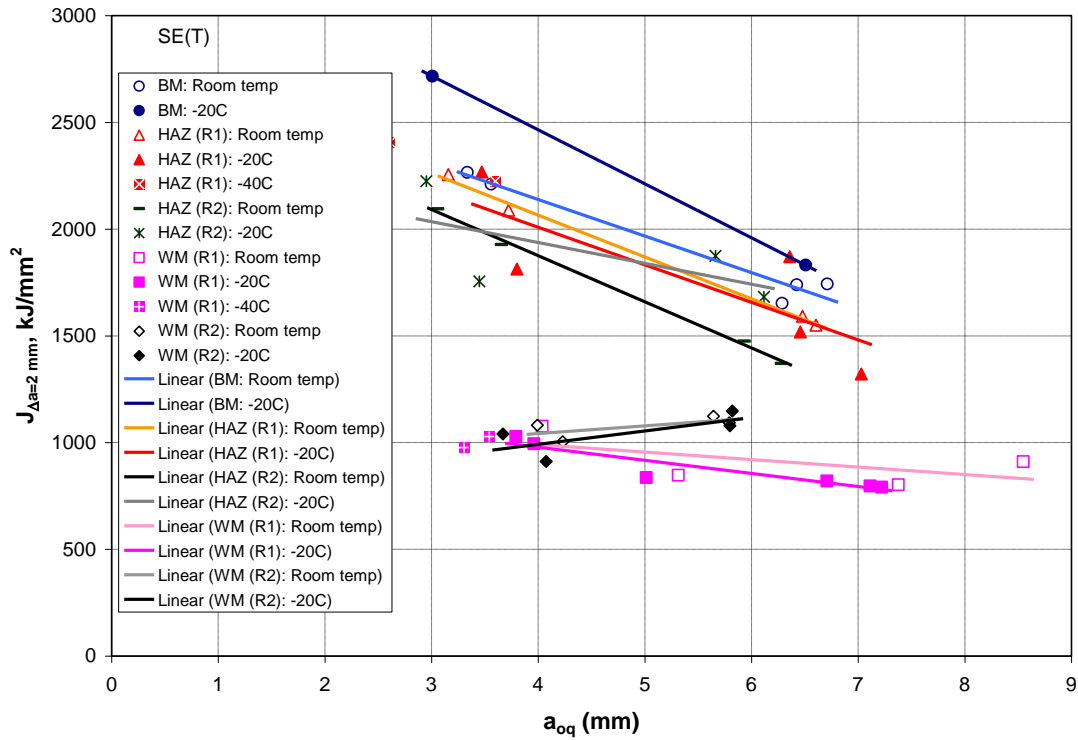


(a)

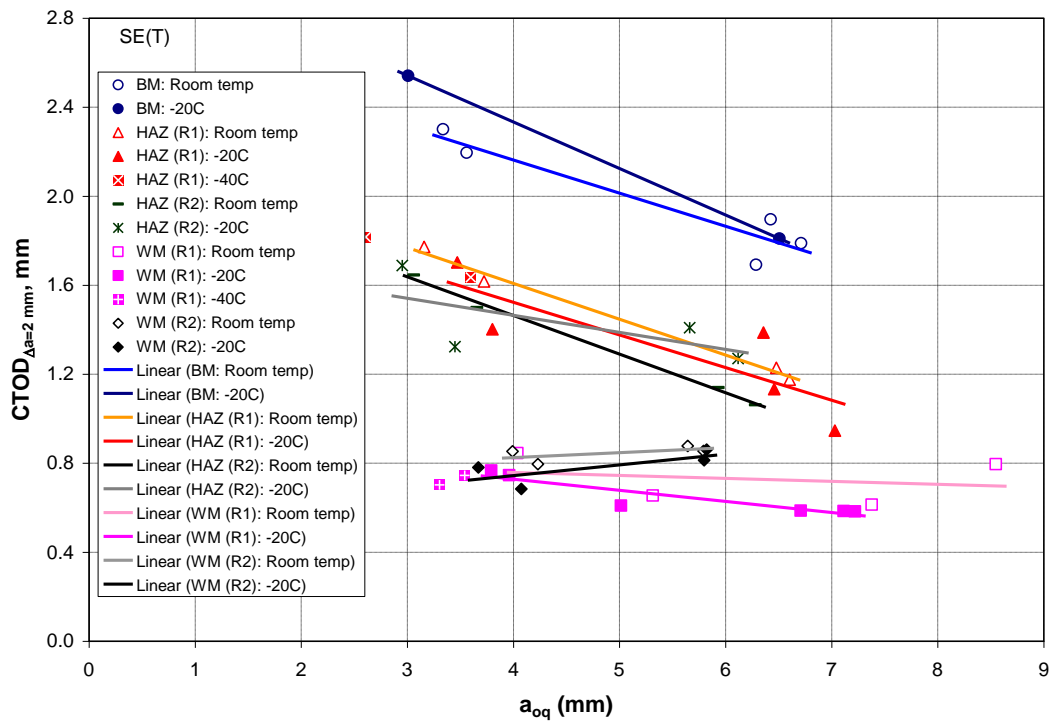


(b)

Figure 25. J and CTOD values at $\Delta a = 0.5$ mm for SE(T): (a) J -resistance and (b) CTOD-resistance.

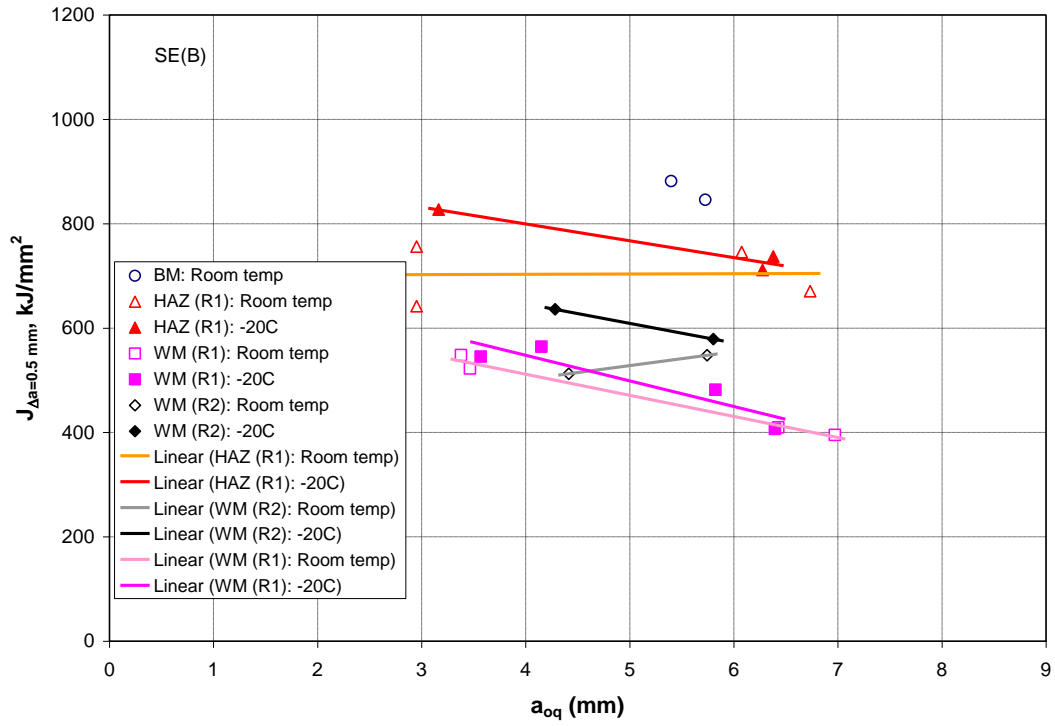


(a)

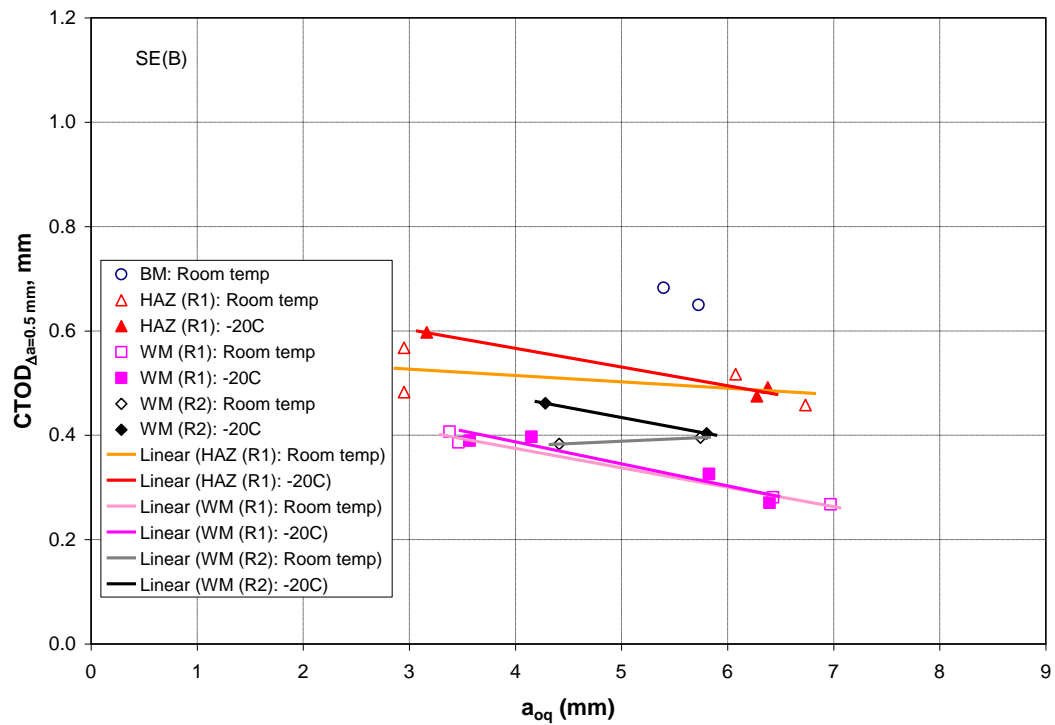


(b)

Figure 26. J and CTOD values at $\Delta a = 2$ mm for SE(T): (a) J -resistance and (b) CTOD-resistance.

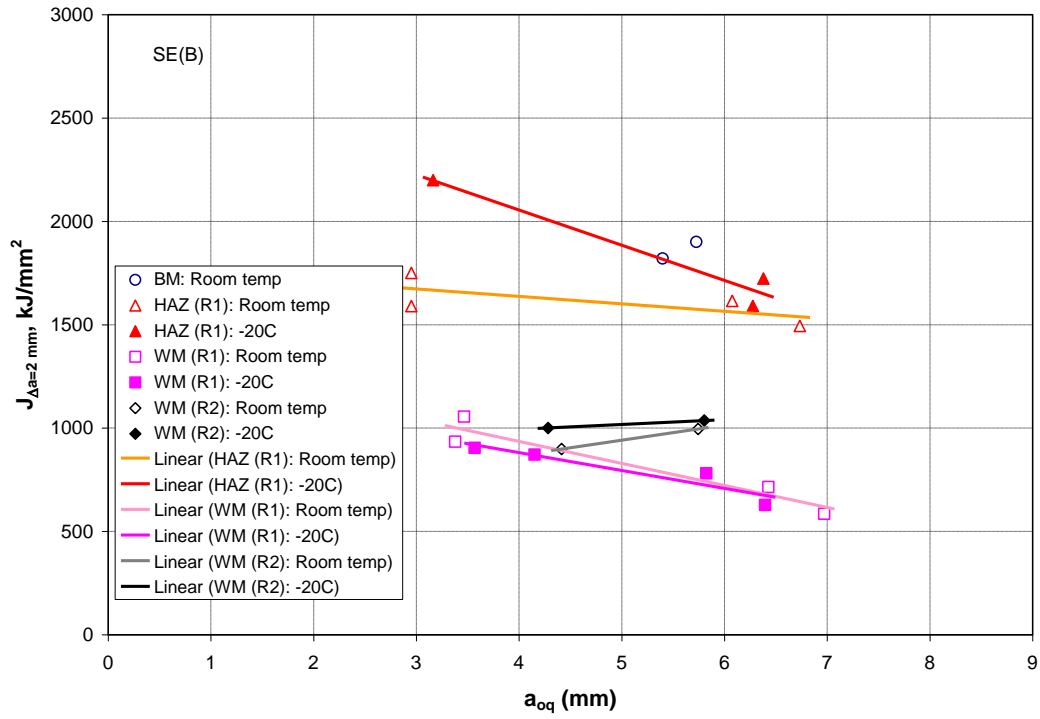


(a)

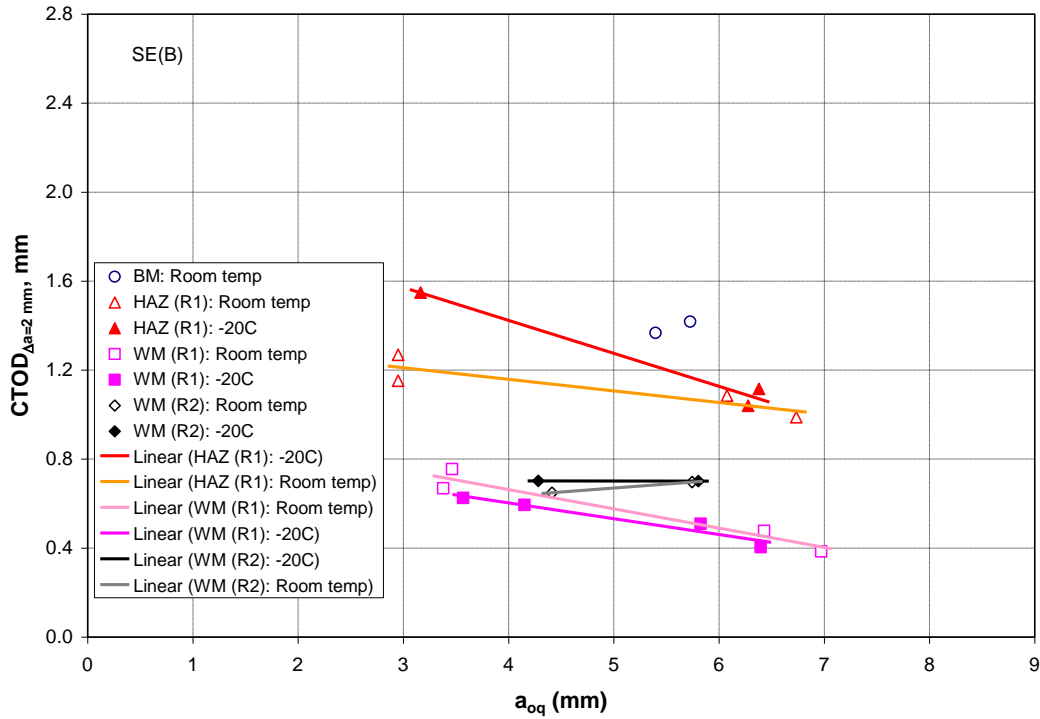


(b)

Figure 27. J and CTOD values at $\Delta a = 0.5 \text{ mm}$ for SE(B): (a) J -resistance and (b) CTOD-resistance



(a)



(b)

Figure 28. J and CTOD values at $\Delta a = 2 \text{ mm}$ for SE(B): (a) J -resistance and (b) CTOD-resistance.

4.6 Asymmetrical Deformation of HAZ Specimens

For HAZ specimens, the BM side deforms more during crack growth for overmatched welds, consequently, the crack growth appears larger on the WM side (Figure 24, Figure 29 and Figure 30): compare HAZ specimens with BM or WM specimens). Optical measurements were made on both the BM and WM sides of the mating fracture surfaces for HAZ specimens. The crack length predicted by unloading compliance is generally closer to the measurement on the WM side than on the BM side because of the relatively severe deformation on the latter (*e.g.*, the circled data shown in Figure 31). However, the compliance prediction fell between the two optical measurements. Owing to the deformation on the BM side, many specimens do not meet the final crack size requirement based on the measurement on the BM side, whereas they meet it when they are measured on the WM side (Table 2).

The asymmetric deformation resulting from the overmatching weld strength is pronounced in SE(T) specimens relative to SE(B) specimens (Figure 29, Figure 30 and Figure 32). This is probably because the stress gradient ahead of the crack tip is higher for SE(B) than SE(T) specimens [10], so that the deformation is more extensive in the SE(T) specimens. Table 2 and Table 3 also show that the final crack length measurements and estimations meet the crack requirement of the ASTM standard on both weld metal side and base metal side for SE(B), but many SE(T) specimens do not fulfill it on the measurements of base metal side.

In an overmatched weld notched in the HAZ, together with the asymmetric deformation, the crack grows toward the lower-strength material (softened HAZ and BM). Figure 24(c) clearly shows the biased crack growth direction as well as the severe deformation on the base metal side. The measured crack extensions on the BM and WM sides are 1.96 mm and 2.06 mm, respectively. The crack tip is approaching the boundary between HAZ and BM in the figure. If it were to grow further, into the BM, the toughness will reflect BM properties rather than those of the HAZ. However, the resistance curve is relevant for engineering critical assessment (ECA), since it reflects the actual growth of a crack initiating in the HAZ. A complicating factor is that, as the crack deviates out of the plane of the side grooves, the assumption of planar crack growth underlying calculations of J and crack size are violated. Figure 33 shows an anomalous resistance curve after crack growth of approximately 4 mm; this may result from errors in the calculation of J and crack growth.

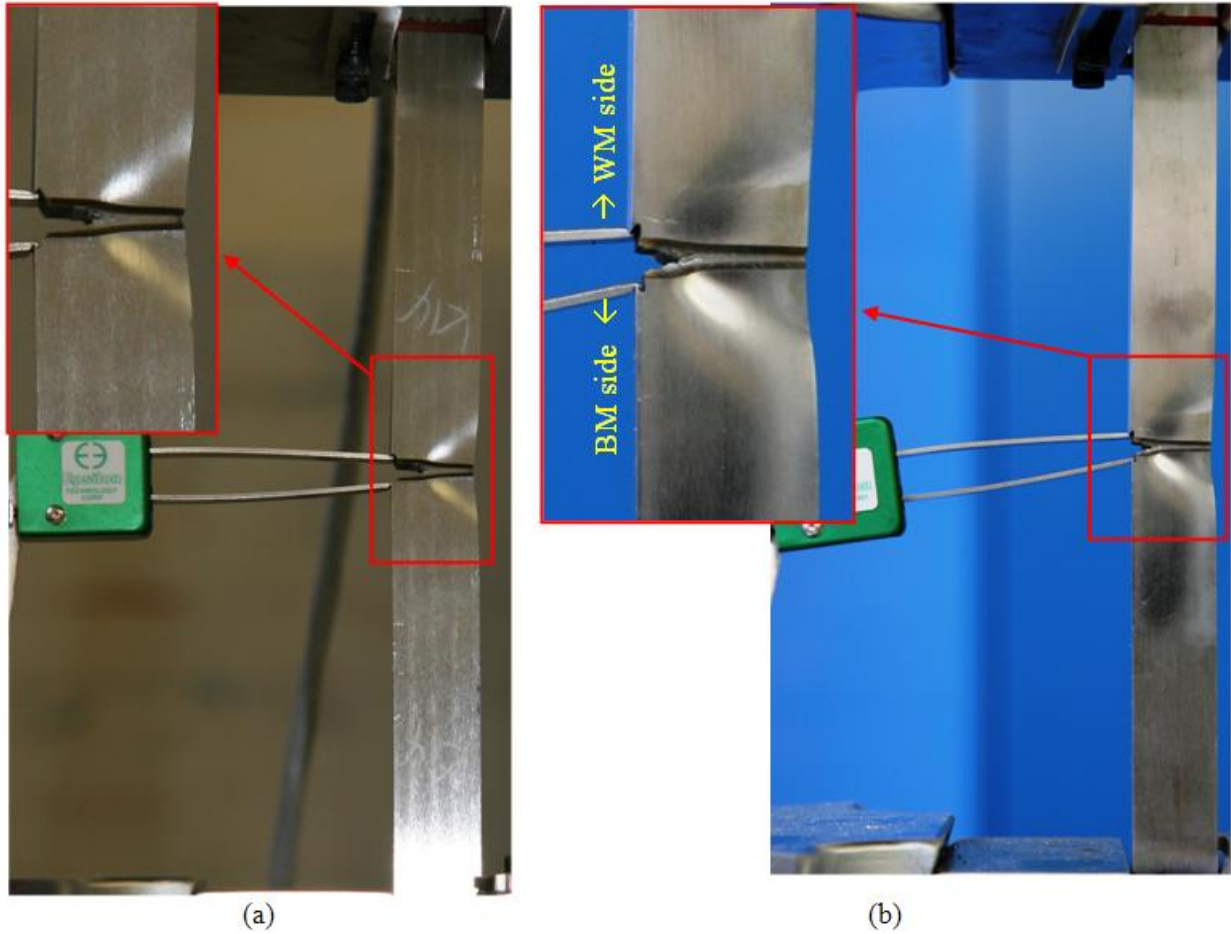
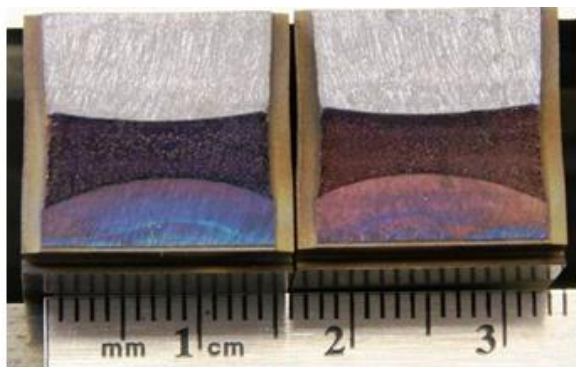
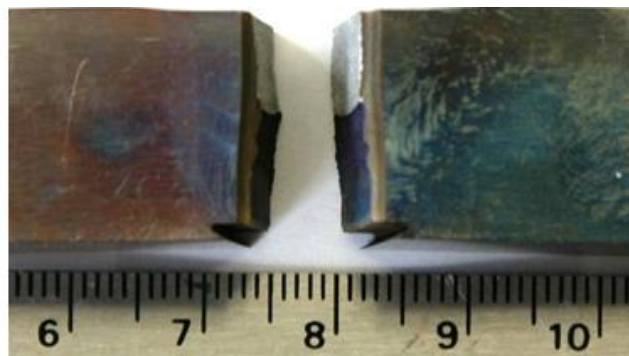


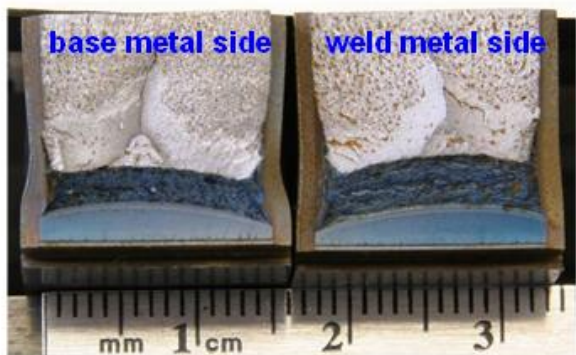
Figure 29. Deformation behaviors during SE(T) testing at CANMET: (a) symmetrical deformation of base metal specimen ($a_o \approx 6$ mm) at $\Delta a \approx 2.5$ mm and (b) asymmetrical deformation between the upper half (WM side) and the lower half (BM side) of a dual-torch weld HAZ specimen ($a_o \approx 3$ mm) at $\Delta a \approx 2.2$ mm.



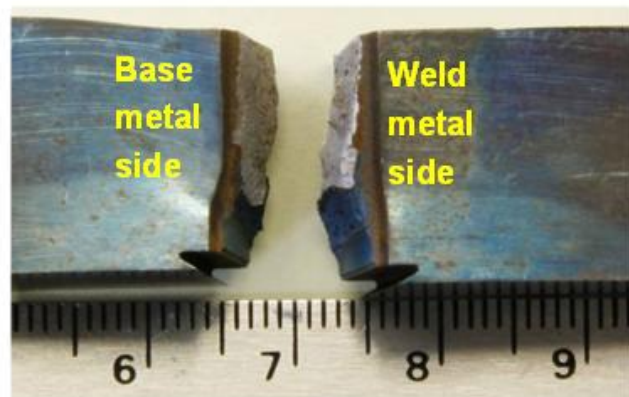
(a)



(b)

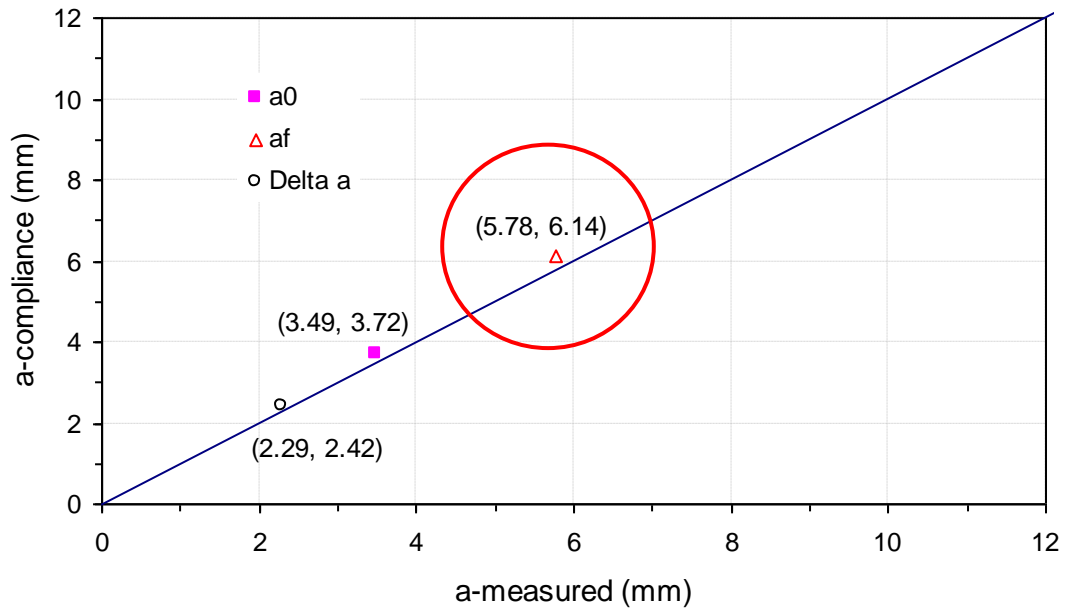


(c)

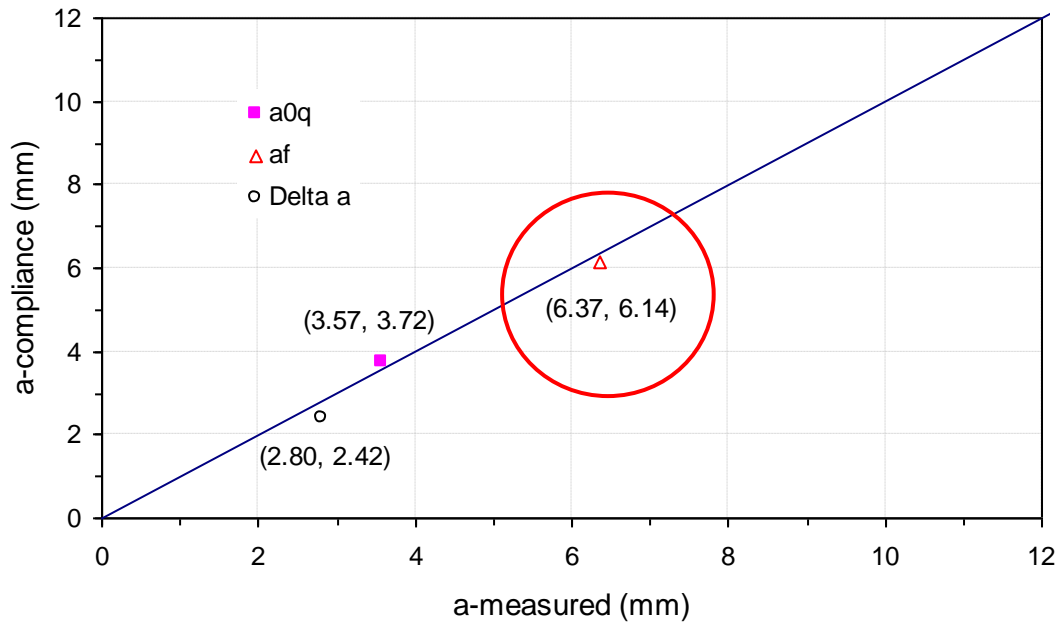


(d)

Figure 30. Examples of fracture surfaces of SE(T) specimens: single-torch weld, nominal $a_o \approx 3$ mm, notched at weld metal centerline (WM) (a) crack plane and (b) side view, and at HAZ (c) crack plane and (d) side view.



(a)



(b)

Figure 31. Effect of overmatching WM for surface notched HAZ specimens: compliance-predicted versus optical crack length measurements of (a) Base metal side and (b) Weld metal side. (Bracketed numbers give optical and compliance measurements, respectively.)

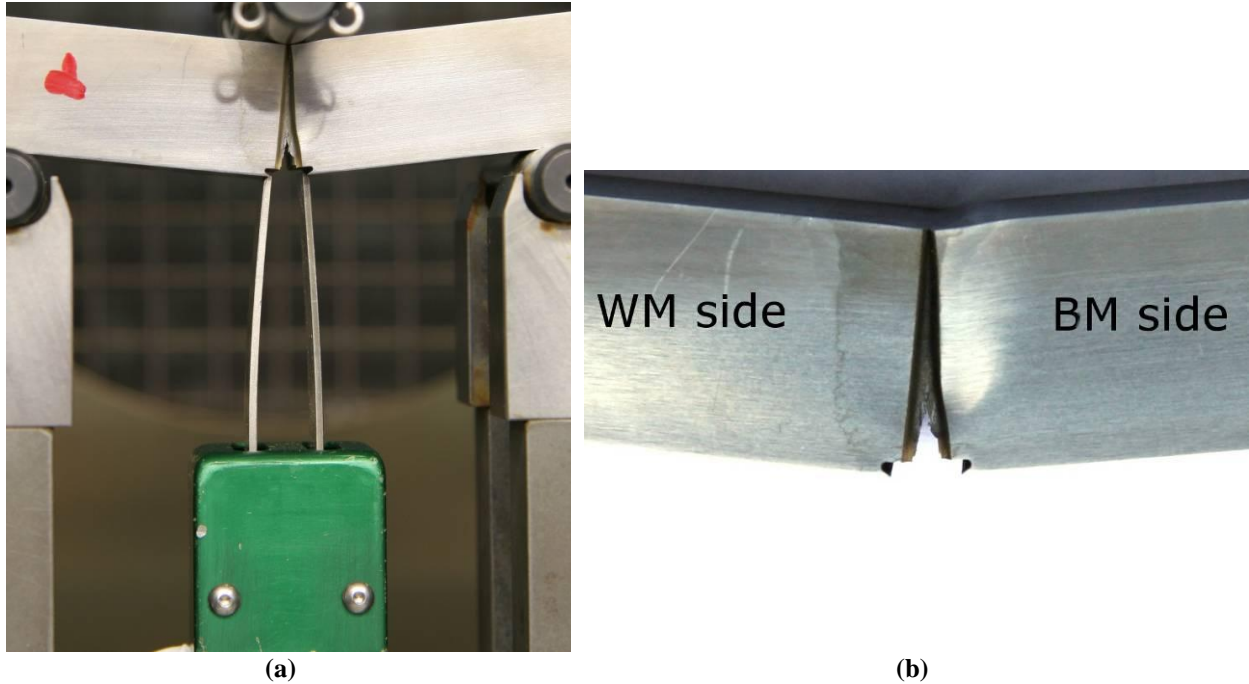


Figure 32. An example of asymmetrical deformation, during SE(B) testing, around the crack tip ($a_0 \approx 3$ mm) precracked in the HAZ region of single-torch weld metal specimen: (a) at $\Delta a \approx 2.4$ mm and (b) after completion of test.

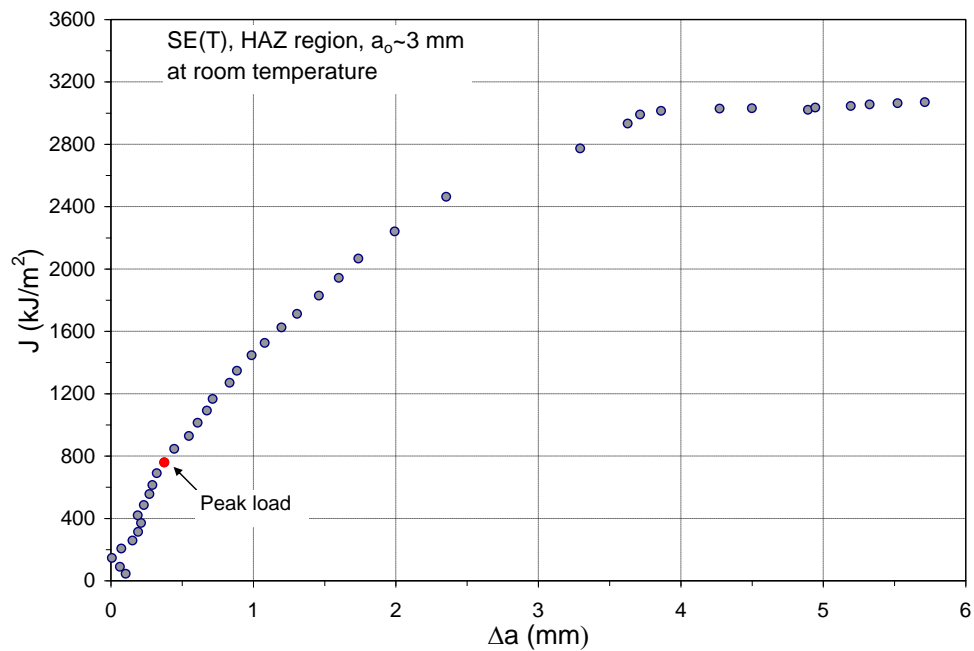


Figure 33. J-resistance curve of a SE(T) HAZ specimen (HZRTK21) carried to exceptionally long crack growth at room temperature.

5 CONCLUSIONS

Extensive SE(T) and SE(B) toughness testing of specimens from X100 pipeline girth welds was conducted, extending the SE(T) procedure developed at CANMET for homogeneous materials to welds. The data was developed for use in interpretation of curved-wide-plate tests carried out in another part of this consolidated program. The intent is to develop strain-based design and assessment procedures for pipeline girth welds. J- and CTOD-resistance curves were derived using the CANMET and ASTM E1820 procedures for SE(T) and SE(B) tests, respectively. The following results and conclusions were obtained:

1. Surface notched specimens produced relatively straight fatigue crack fronts both without (round 1 & round 2) and with (round 3) local compression prior to precracking.
2. The optimal side grooves were 15 %B (depth of 7.5 %B on each side), where B is the thickness of the specimen. A total side-grooving depth of 10 % (5 %B on each side) was used for round 3 specimens and appears to have little or no effect on test results, as confirmed by the comparison with one plane-sided SE(T) specimen.
3. Resistance R curves for weld metal (WM) were lower than those for base metal (BM) or heat-affected zone (HAZ) specimens, even though the WM overmatched the BM. Toughness properties for round 3 welds were superior to those for rounds 1 and 2 weld metals, although a difference in pipe wall thickness could moderate this conclusion.
4. Power-law regression curves generated for data between exclusion lines (following ASTM procedures) adequately represented data measured for significantly larger crack growth, *i.e.*, within 10 % error for an approximate doubling of crack growth.
5. Toughness of BM, HAZ and WM increased significantly with decreases in initial crack length, although R-curves for dual-torch WM (R2) were relatively insensitive to initial crack length.
6. In an overmatched weld notched in the HAZ, asymmetric deformation occurs at the crack tip and leads to biased crack growth and discrepancy in crack length measurements on the BM and WM sides. The crack grows toward the lower-strength base metal, and the change in crack length Δa tends to be larger on the WM side for overmatched welds.

6 ACKNOWLEDGEMENTS

This work is part of a larger consolidated program jointly funded by the Canadian Federal Government Program of Energy Research and Development (PERD), the Pipeline and Hazardous Materials Safety Administration of the U.S. Department of Transportation (DOT), and the Pipeline Research Council International, Inc. (PRCI).

7 REFERENCES

1. Shen, G and Tyson, WR. “*Crack length evaluation for SE(T) testing using unloading compliance,*” Journal of Testing and Evaluation, 37: 347-357, 2009.
2. Shen, G., Gianetto, J.A, And Tyson, W.R., “*Development Of Procedure For Low-Constraint Toughness Testing Using A Single-Specimen Technique*”, Final Report 277-T-03 To PHMSA Per Agreement # DtpH56-07-T-000005, September 2011.
3. Shen, G, Gianetto, JA And Tyson, WR, “*Measurement Of J-R Curves Using Single-Specimen Technique On Clamped SE(T) Specimens*”, Proceedings Of The 19th ISOPE Conference, Osaka, Japan, June-21-26, 2009.
4. ASTM E1820-11, *Standard Test Method For Measurement Of Fracture Toughness*, ASTM International, U.S.A, 2011.
5. Park, D.Y., Tyson, W.R., Gianetto, J.A., Shen, G., Eagleson, R.S., Lucon, E. And Weeks, T.S., “*Small Scale Low Constraint Fracture Toughness Test Results*”, Final Report 277-T-06 To PHMSA Per Agreement # DTPH56-07-T-000005, September 2011.
6. Gianetto, J., Tyson, W.R., Park, D.Y., Shen, G., Lucon, E., Weeks, T.S., Quintana, M.A., Rajan, V.B. And Y-Y Wang, “*Small Scale Tensile, Charpy V-Notch, And Fracture Toughness Tests*”, Final Report 277-T-05 To Phmsa Per Agreement # DtpH56-07-T-000005, September 2011.
7. British Standard BS 7448, *Fracture Mechanics Toughness Tests*, British Standards Institution, London, England, 1997.
8. Park, D-Y, Tyson, WR, Gianetto, JA, Shen, G and Eagleson, RS. “*Evaluation of Fracture Toughness of X100 Pipe Steel Using SE(B) and Clamped SE(T) Single Specimens,*” Proceedings of 8th International Pipeline Conference, IPC 2010, Calgary, Canada, September 2010.
9. Shen, G, Tyson, WR, Gianetto, JA, and Park, D-Y., “*Effect of Side Grooves on Compliance, J-integral and Constraint of a Clamped SE(T) Specimen*”, Proceedings of PVP 2010, ASME Pressure Vessel and Piping Division Conference, Seattle, USA, July 2010.
10. Shen, G, Bouchard, R, Gianetto, JA and Tyson, WR., “*Fracture toughness evaluation of high strength steel pipe*”, Proceedings of PVP2008, ASME Pressure Vessel and Piping Division Conference, Chicago, Illinois, USA, 2008.
11. Anon., *Fracture Control for Pipeline Installation Methods Introducing Cyclic Plastic Strain*, Recommended Practice DNV- RP-F108, Det Norske Veritas, January 2006.
12. Tyson, WR, Park, D-Y and Shen, G., “*Improved crack growth correction for resistance curve determination,*” Proceedings of ECF18, 18th European Conference on Fracture, Dresden, Germany, Aug. 2010.
13. Wei, S, Lu, S, Li, D and Li, Y., “*Impact property analysis of weld metal and heat-affected zone for low-alloy carbon steel multi-pass welded joint,*” China Welding (English Edition), 19, 21-25, 2010.